

# Reviewing the prospect of fermion triplets as dark matter and source of baryon asymmetry in non-standard cosmology

Anirban Biswas,<sup>a,b</sup> Mainak Chakraborty,<sup>c</sup> Sarif Khan<sup>d</sup>

<sup>a</sup>Department of Physics & Lab of Dark Universe, Yonsei University, 50 Yonsei-ro, Seodaemun-gu, Seoul 03722, South Korea

<sup>b</sup>Center for Quantum Spacetime, Sogang University, 35 Baekbeom-ro, Mapo-gu, Seoul 121-742, South Korea

<sup>c</sup>School of Physical Sciences, Indian Association for the Cultivation of Science, 2A & 2B Raja S.C. Mullick Road, Kolkata 700 032, India

<sup>d</sup>Institut für Theoretische Physik, Georg-August-Universität Göttingen, Friedrich-Hund-Platz 1, 37077 Göttingen, Germany

E-mail: [anirban.biswas.sinp@gmail.com](mailto:anirban.biswas.sinp@gmail.com), [psmc2382@iacs.res.in](mailto:psmc2382@iacs.res.in), [sarif.khan@uni-goettingen.de](mailto:sarif.khan@uni-goettingen.de)

**Abstract.** Indirect searches of Dark Matter (DM), in conjugation with ‘missing track searches’ at the collider seem to confine  $SU(2)_L$  fermion triplet DM (FTDM) mass within a narrow range around 1 TeV. The canonical picture of the pure FTDM is in tension since it is under-abundant for the said mass range. Several preceding studies have reported that an extra species ( $\phi$ ), redshifts faster than the radiation ( $\sim a^{-(4+n)}$  where  $n > 0$ ), leads to a faster expanding early Universe by dominating in the energy density with an enhanced Hubble parameter. This has the potential to revive the under-abundant FTDM ( $\mathbb{Z}_2$  odd, lightest generation) by causing freeze-out earlier without modifying the interaction strength between DM and thermal bath. On the other hand, although the CP asymmetry produced due to the decay of  $\mathbb{Z}_2$  even heavier generations of the triplet remains unaffected, its evolution is greatly affected by the non-standard cosmology. It has been observed through numerical estimations that the minimum mass of the triplet, required to produce sufficient baryon asymmetry of the Universe (BAU), can be lowered up to two orders (compared to the standard cosmology) in this fast expansion scenario. The non-standard parameters  $n$  and  $T_r$  (a reference temperature below which radiation dominance prevails), which simultaneously control DM abundance as well as the frozen value of BAU, are tightly constrained from the observed experimental values. We have found that  $n$  is strictly bounded within the interval  $0.4 \lesssim n \lesssim 1.8$  where the upper bound is imposed by the BAU constraint whereas the lower bound arises to satisfy the correct DM abundance. It has been noticed that the restriction on  $T_r$  is not so stringent as it can vary from sub GeV to a few tens of GeV.

---

## Contents

<b>1</b>	<b>Introduction</b>	<b>2</b>
<b>2</b>	<b>Model</b>	<b>4</b>
<b>3</b>	<b>Type III Seesaw explaining neutrino mass</b>	<b>6</b>
<b>4</b>	<b>Lightest triplet as DM candidate</b>	<b>7</b>
4.1	Constraints on triplet DM	7
4.2	Evolution of comoving number density in non-standard cosmology	9
4.2.1	Determining the freeze-out temperature $T_f$	11
4.2.2	Analytical approximation for DM relic density	12
4.2.3	BBN Bound	13
4.3	Numerical results: viability of fermion triplet DM	14
4.3.1	Graphical analysis of numerical results	14
<b>5</b>	<b>Baryogenesis through Type-III seesaw leptogenesis</b>	<b>20</b>
5.1	CP asymmetry	21
5.2	Boltzmann equations for leptogenesis in standard cosmology	23
5.2.1	Baryon asymmetry and efficiency factor at present epoch	25
5.2.2	Modification of the Boltzmann equations in non-standard cosmology	25
5.3	Analysis of numerical results: constraining the non-standard parameters	26
<b>6</b>	<b>Summary and Conclusion</b>	<b>30</b>
<b>A</b>	<b>Thermal averaged cross-section</b>	<b>32</b>
<b>B</b>	<b>Equilibrium number density and freeze-out temperature</b>	<b>32</b>
<b>C</b>	<b>Reaction densities of various decay, inverse decay, scattering processes</b>	<b>33</b>
<b>D</b>	<b>Scattering cross-section of various processes</b>	<b>34</b>

---

# 1 Introduction

The origin of dark matter(DM) and the explanation of the observed matter-antimatter asymmetry are two most important and unresolved issues in particle and astroparticle physics. The existence of dark matter has been suggested by a plethora of observations at the galactic scale like galactic rotation curves [1], gravitational lensing of distant celestial bodies [2], colliding galaxy clusters (e.g. the Bullet cluster) [3] etc. Similarly, the observations at the cosmological scale by WMAP [4] and Planck [5, 6] satellites have measured most precisely the abundance of dark matter till date,  $\Omega_{\text{DM}}h^2 = 0.120 \pm 0.001$  at 68% C.L. [6], which is roughly around 25% energy budget of our Universe. While Weakly Interacting Massive Particle (WIMP) [7–10] characterised by the GeV–TeV scale mass window with weak scale interaction cross-section is one of the most preferred dark matter candidates, there exist various other possibilities like, non-thermal dark matter [11–13], asymmetric dark matter [14], primordial black hole as dark matter [15] etc. On the other hand, there are overwhelming evidences in support of excess baryonic matter over anti-matter at various cosmological epochs. The baryon-to-photon ratio ( $\eta_B$ ) predicted during the Big bang nucleosynthesis (BBN) by measuring various light element abundances matches excellently with that obtained from the baryon density at the time of recombination. The current acceptable value of  $\eta_B$  which carries the information about the baryon asymmetry<sup>1</sup> of the Universe (BAU) is  $\eta_B = (6.4 \pm 0.1) \times 10^{-10}$  at 95% C.L. [6]. Non-zero neutrino masses and large leptonic mixing [16, 17] have now become experimentally [18–25] verified fact and the experiments are now inching towards precise measurement of the oscillation parameters [26]. Various seesaw mechanisms [27–32], introduced to explain tiny mass of the active neutrinos, can act as a bridge between DM phenomenology and mechanism of dynamical generation of baryon asymmetry through lepton asymmetry(popularly known as Baryogenesis via Leptogenesis [33]).

In this work, we have considered one of the minimal extensions of the SM to address both the dark matter and the baryon asymmetry of the Universe. Here we have added three  $\text{SU}(2)_L$  fermionic triplets with hypercharge  $Y = 0$  in the particle spectrum of the SM. As a result, two of the three light neutrinos have sub-eV Majorana masses through the Type-III seesaw mechanism and the remaining one continues to be massless due to the imposition of an additional  $\mathbb{Z}_2$  odd parity on the lightest triplet fermion  $\Sigma_{R1}$ . Accordingly, the triplet  $\Sigma_{R1}$  gets decoupled from the neutrino sector and its neutral component  $\Sigma_1^0 (= \Sigma_{R1}^0 + \Sigma_{R1}^{0c})$  could be a Majorana type dark matter candidate which satisfies the relic density bound for  $M_{\Sigma_1} \simeq 2.3$  TeV [34]. However, such a dark matter candidate in the mass range  $1.5 \text{ TeV} \lesssim M_{\Sigma_1} \lesssim 2.7 \text{ TeV}$  is already ruled out by the indirect detection bound coming from dark matter annihilation into  $W^+W^-$  and  $\gamma\gamma$  final states [35, 36]. There are some earlier attempts to generate correct relic abundance for the low mass triplet fermionic dark matter by either introducing an additional non-thermal contribution to the relic density from a decaying scalar [37] or including a singlet fermion with a nonzero mixing with the triplet such that the resulting dark matter candidate is predominantly a singlet-like state [38]. In this work, we are considering another interesting way to bring relic density in the correct ballpark value of Planck collaboration [6] in the low mass regime of the triplet dark matter. Here, we modify the underlying cosmology of the early<sup>2</sup> Universe by adding

---

<sup>1</sup>It is to be noted that baryon asymmetry can also be expressed as net baryon number density scaled by entropy density i.e  $Y_B = \frac{n_B}{s}$  and its experimental value lies within  $(9.05 \pm 0.150) \times 10^{-11}$ .

<sup>2</sup>The word ‘early’ signifies an era which started earlier than the thermal production scale of heavy fermion triplets and lasts till the freeze-out epoch of the DM.

extra species which redshifts faster than the radiation content of the Universe. There is a large ambiguity about the cosmology of the Universe prior to the era of light nuclei (H, D,  $^3\text{He}$ ,  $^4\text{He}$ , and  $^7\text{Li}$ ) formation, popularly known as the Big bang nucleosynthesis which began when the age of the Universe was  $\sim 1$  second and it continued for about three minutes. More importantly, the theoretical predictions of BBN (e.g. light nuclei abundance), considering radiation dominated Universe, are in good agreement with observational data. On the contrary, very little information is available to us about the era before BBN and in most of the literature a radiation dominated Universe has been considered. However, the expansion rate of the Universe driven by the Hubble parameter can be higher or lower compared to the case of radiation domination depending on how the total energy density of the Universe redshift with respect to expansion. The fast expansion results if there is an additional source of energy on top of the radiation background composed of the SM particles such that the total energy density  $\rho_{\text{tot}} > \rho_{\text{rad}}$ , the energy density due to radiation. The early matter domination [39–42], the kination [43–48] etc. are a few examples of fast expanding Universe. On the other hand, the opposite situation could also arise particularly in some modified gravity theory [49–53] where a negative contribution in the energy density leads to slow expansion [54].

In this work, we consider a fast expanding Universe by introducing a species  $\phi$  that dominates the energy density in the early Universe. Moreover, the energy density of  $\phi$  red-shifts at a faster rate with the cosmic scale factor ( $a$ ) compared to that of the radiation ( $\rho_{\text{rad}} \propto a^{-4}$ ) i.e.  $\rho_{\phi} \propto a^{-(4+n)}$  with  $n > 0$ . Therefore, although initially we have  $\phi$  dominance, the radiation eventually takes over from  $\phi$  before the start of BBN ( $T \sim 1$  MeV) since the latter decreases rapidly due to expansion. The revival of radiation domination is characterised by the temperature  $T_r \geq 1$  MeV. Accordingly, we have two new parameters  $n$  and  $T_r$  (both are not independent) controlling the cosmology of the Universe for  $T > T_r$ . Depending upon the value of  $n$  we can have different expansion histories of the Universe. For example, the scenario with  $n = 2$  can be realised if the kinetic energy of a scalar field dominates the energy budget, which is known as the Kination era where  $\rho_{\phi} \propto a^{-6}$  [45–48]. This simple model for non-standard cosmology was first proposed in [48] and thereafter a number of works have been done using this model in the context of dark matter [55–60] and leptogenesis [61–67]. In this work, our prime motivation is to find an allowed parameter space for the pure triplet dark matter which otherwise is entirely ruled out by the combination of relic density and indirect detection bounds for the standard cosmological scenario. In the radiation dominated Universe, a triplet fermion of mass lower than 2.3 TeV remains under abundant due to large annihilation and co-annihilation cross-sections into electroweak gauge bosons and fermions, which results in a late freeze-out. However, this situation can be changed in presence of a fast expanding Universe characterised by a Hubble parameter larger than the standard scenario. Moreover, the non-standard cosmology also affects the final baryon asymmetry produced from lepton asymmetry through sphaleron involving processes before the electroweak phase transition. In this model the other two heavier triplet fermions, which are even under  $\mathbb{Z}_2$  symmetry, have non-vanishing Yukawa couplings with Lepton doublets and Higgs doublet. Accordingly, the lepton asymmetry can be generated due to CP violating out of equilibrium decays of these heavy triplet fermions at very high temperature. This has been studied earlier considering a radiation dominated Universe before the BBN and found [68–70] that the minimum mass of triplet fermion required to generate the observed baryon asymmetry is  $M_{\Sigma} \gtrsim 3 \times 10^{10}$  GeV. In the present work, we explore the possibility of relaxing the

above mentioned lower bound<sup>3</sup> on  $M_\Sigma$  obtained from BAU bound. Predominance of the extra scalar field  $\phi$  in the primordial Universe resulted in faster (than standard cosmology) expansion of the Universe. Thus enhancement caused in the Hubble parameter pushes the rate of decay/Inverse decay (of  $\Sigma_2$  or  $\Sigma_3$ ) and scattering towards a lower value. Therefore the Boltzmann equations governing the evolution of produced asymmetry will be altered with respect to its standard counterpart. Although the modification of cosmology doesn't affect the asymmetry production, it has non-trivial effect in the evolution of the same. Our aim in this part of the work is to identify the specific region of the parameter space which can produce observed baryon asymmetry below the limit (on the decaying triplet mass) set using standard cosmology.

The fascinating feature of this study is that the newly introduced non-standard cosmology co-relates the apparently decoupled dark sector and the Yukawa sector (responsible CP asymmetry generation) through the non-standard parameters  $T_r, n$ . We expect that the relic density bound together with the observed BAU bound will allow a strongly constrained parameter space spanned by the yet unbounded non-standard parameters  $T_r - n$ .

To address the issues raised in the preceding paragraphs in a comprehensive and systematic manner, the rest of this paper is organized as follows. The minimal extension scheme of SM adopted here, to account for the DM relic abundance as well as the BAU, is discussed in Sec. 2. A qualitative overview about the generation of active neutrino mass and mixing through Type-III seesaw mechanism is presented in Sec. 3. Sec. 4 is solely devoted to the study of DM-phenomenology. Its different subsections are arranged chronologically so that the need for introduction of non-standard cosmology to save the fermion triplet DM scenario can be clearly understood. So we start with a comprehensive analysis of existing bounds (obtained from indirect searches and collider experiments) on fermion triplet DM in sec. 4.1. The collective results allow only a window for triplet DM mass, which is not enough to produce adequate relic abundance in standard cosmological scenario. Thus non-standard cosmology is introduced in Sec. 4.2 and its subsections discuss how the freeze-out temperature of the DM can be modified (Sec. 4.2.1) in the newly introduced cosmology, without harming the successful predictions of the BBN (Sec. 4.2.3). Sec. 4.3 presents a detailed account of numerical analysis related to the study of DM phenomenology in modified cosmological scenario. Sec. 5 contains a rigorous analysis of Baryogenesis through Leptogenesis in the present scenario. Discussions about Leptogenesis, continue in its constituent subsections, starting with generation of CP asymmetry due to the decay of next to lightest triplet (Sec. 5.1), followed by a thorough description of the Boltzmann equations in the non-standard (Sec. 5.2) cosmology and ends with a meticulous analysis (Sec. 5.3) of numerical results supplemented by plots of suitable model parameters. The noteworthy outcomes of this exhaustive study are summarised in Sec. 6.

## 2 Model

In the present work, we have addressed a few well-recognised SM drawbacks namely dark matter, neutrino mass and matter anti-matter asymmetry of the Universe. To this end, we have extended the SM particle content by three additional  $SU(2)_L$  triplet fermions similar to the Type-III seesaw mechanism. The complete particle spectrum with the associated charge assignment is shown in Table 1. Among them, the lightest one is  $\mathbb{Z}_2$  odd and its

---

<sup>3</sup>One can also lower the triplet mass bound by extending the minimal model with additional fields as done in [71].

neutral component serves as the suitable DM candidate whereas the other two are  $\mathbb{Z}_2$  even and contribute to the neutrino mass through the Type-III seesaw mechanism. We have considered its ( $\Sigma_1$ ) mass in the TeV range. Fermion triplet DM heavier than 2.4 TeV is ruled out by Planck data due to the over-abundance. Moreover, for mass beyond 1.5 TeV, DM annihilation faces Sommerfeld enhancement [35, 36] which is in direct contradiction with the indirect detection bound provided by Fermi-LAT data [72]. Therefore, we have considered  $\Sigma_1$  mass always below 1.5 TeV. This mass restriction forbids the lightest fermion triplet to account for the full relic abundance of DM as reported by the experiments. We also discuss in the result section, how the presence of an extra species (denoted as  $\phi$ ) in the early Universe assist us to obtain the total amount of dark matter relic density even below 1 TeV, which was not possible in standard cosmological scenario. The other two triplet fermions, which are even under  $\mathbb{Z}_2$  symmetry, take part in the generation of neutrino mass, lepton asymmetry, are kept at a very high scale  $\mathcal{O}(10^9)$  GeV. The improvement of the lower bound on triplet mass, to obtain the correct value of BAU, due to the presence of the extra species in the early Universe is emphasized in the section dedicated to ‘Baryogenesis through Leptogenesis’.

Gauge Group	Quarks			Leptons				Scalar
	$Q_L^i = (u_L^i, d_L^i)^T$	$u_R^i$	$d_R^i$	$L_L^i = (\nu_L^i, e_L^i)^T$	$e_R^i$	$\Sigma_{Rj}^c$	$\Sigma_{R1}^c$	$\Phi$
$SU(2)_L$	2	1	1	2	1	3	3	2
$U(1)_Y$	1/6	2/3	-1/3	-1/2	-1	0	0	1/2
$\mathbb{Z}_2$	1	1	1	1	1	1	-1	1

**Table 1.** Particle contents and their corresponding charges under the SM gauge group.

The Lagrangian for the particle spectrum shown in Table 1 is given by,

$$\mathcal{L} = \mathcal{L}_{\text{SM}} + \mathcal{L}_{\Sigma}, \quad (2.1)$$

where  $\mathcal{L}_{\text{SM}}$  is the Lagrangian associated with the SM particles and  $\mathcal{L}_{\Sigma}$  is the Lagrangian for the triplet fermions which has the following form,

$$\begin{aligned} \mathcal{L}_{\Sigma} = & \frac{i}{2} \sum_{j=1,2,3} \text{Tr} \left[ \overline{\Sigma_{Rj}} \not{D} \Sigma_{Rj} + \overline{\Sigma_{Rj}^c} \not{D} \Sigma_{Rj}^c \right] - \sum_{\alpha=1}^3 \sum_{j=1}^3 \left( \sqrt{2} y_{\Sigma}^{\alpha j} \overline{L_{L\alpha}} \Sigma_{Rj} \tilde{\Phi} + h.c. \right) \\ & - \frac{1}{2} \sum_{j=1}^3 \text{Tr} \left[ \overline{\Sigma_{Rj}^c} (M_{\Sigma})_{jj} \Sigma_{Rj} + h.c. \right], \end{aligned} \quad (2.2)$$

where the above three terms are, respectively, the kinetic term, the Yukawa coupling term and the bare mass term for the fermion triplets  $\Sigma_j$  ( $j = 1, 2, 3$ ). The Latin index  $j = 1$  to 3 stands for three generations of fermion triplets whereas the Greek index  $\alpha$  is used to designate three different lepton flavours. It is to be noted that although the summation on  $j$  runs from 1 to 3 in the second term, the species  $\Sigma_{R1}$  does not couple to the SM Higgs and the lepton doublets, which implies that the first column of the Yukawa coupling matrix  $y_{\Sigma}$  is null. This has been implemented by imposing a  $\mathbb{Z}_2$  odd parity to the lightest triplet generation *i.e.*  $\Sigma_{R1}$  whereas all the other species are  $\mathbb{Z}_2$  even including the SM particles. It should be noted that we have constructed the physical basis using a linear combination of component field and its

CP conjugate of each triplet  $\Sigma_{Rj}$ . In the fundamental representation of  $SU(2)_L$ , the triplet  $\Sigma_{Rj}$  can be expressed as

$$\Sigma_{Rj} = \begin{pmatrix} \Sigma_{Rj}^0/\sqrt{2} & \Sigma_{Rj}^+ \\ \Sigma_{Rj}^- & -\Sigma_{Rj}^0/\sqrt{2} \end{pmatrix}. \quad (2.3)$$

The  $2 \times 2$  representation of  $\Sigma_{Rj}$  transforms under  $SU(2)_L$  as  $\Sigma'_{Rj} = U \Sigma_{Rj} U^\dagger$  with  $U = \exp(-i \frac{g}{2} \theta_a \sigma_a)$  and  $\sigma_a$  ( $a = 1, 2, 3$ ) are the Pauli matrices. The complex conjugate of  $\Sigma_{Rj}$ ,  $\Sigma_{Rj}^*$ , does not transform in the similar manner as  $\Sigma_{Rj}$  under  $SU(2)_L$ . However, the combination  $i\sigma_2 \Sigma_{Rj}^* i\sigma_2$  has the identical transformation property as that of the triplet  $\Sigma_{Rj}$ . Therefore, in order to have an  $SU(2)$  invariant Lagrangian, the CP conjugate of triplet  $\Sigma_{Rj}$  is defined as

$$\Sigma_{Rj}^c = i\sigma_2 C \overline{\Sigma_{Rj}}^T i\sigma_2 = \begin{pmatrix} \Sigma_{Rj}^{0c}/\sqrt{2} & \Sigma_{Rj}^{-c} \\ \Sigma_{Rj}^{+c} & -\Sigma_{Rj}^{0c}/\sqrt{2} \end{pmatrix}. \quad (2.4)$$

Nevertheless, the CP conjugates of the component fields follow the usual definition i.e.  $\Sigma_{Rj}^0 = C \overline{\Sigma_{Rj}^0}^T$  and  $\Sigma_{Rj}^\pm = C \overline{\Sigma_{Rj}^\pm}^T$ . Now, using both  $\Sigma_{Rj}$  and  $\Sigma_{Rj}^c$ , we can construct a triplet for each generation as

$$\begin{aligned} \Sigma_j &= \Sigma_{Rj} + \Sigma_{Rj}^c \\ &= \begin{pmatrix} \Sigma_j^0/\sqrt{2} & \Sigma_j^+ \\ \Sigma_j^- & -\Sigma_j^0/\sqrt{2} \end{pmatrix}, \end{aligned} \quad (2.5)$$

where, the neutral parts  $\Sigma_j^0 = \Sigma_{Rj}^0 + \Sigma_{Rj}^{0c}$  are the Majorana fermions while the charged parts  $\Sigma_j^\pm = \Sigma_{Rj}^\pm + \Sigma_{Rj}^{\mp c}$  are the Dirac fermions. In terms of newly defined fields  $\Sigma_j^0$  and  $\Sigma_j^\pm$ , the Lagrangian given in Eq. (2.2) takes the following form [37]

$$\begin{aligned} \mathcal{L}_\Sigma &= i \overline{\Sigma_j^-} \not{\partial} \Sigma_j^- + \frac{i}{2} \overline{\Sigma_j^0} \not{\partial} \Sigma_j^0 - M_{\Sigma_j} \overline{\Sigma_j^-} \Sigma_j^- - \frac{M_{\Sigma_j}}{2} \overline{\Sigma_j^0} \Sigma_j^0 - g \left( \overline{\Sigma_j^-} W^- \Sigma_j^0 + h.c. \right) \\ &\quad + g \cos \theta_W \overline{\Sigma_j^-} Z \Sigma_j^- + g \sin \theta_W \overline{\Sigma_j^-} A \Sigma_j^- - \sqrt{2} \left\{ y_\Sigma^{\alpha j} \left( \frac{1}{\sqrt{2}} \overline{\nu_{L\alpha}} P_R \Sigma_j^0 + \overline{\ell_{L\alpha}} P_R \Sigma_j^- \right) H^{0*} \right. \\ &\quad \left. - y_\Sigma^{\alpha j} \overline{\nu_{L\alpha}} P_R \Sigma_j^+ H^- + \frac{y_\Sigma^{\alpha j}}{\sqrt{2}} \overline{\ell_{L\alpha}} P_R \Sigma_j^0 H^- + h.c. \right\}. \end{aligned} \quad (2.6)$$

Here,  $H^-$  and  $H^0$  are charged and neutral components of the Higgs doublet  $H$  respectively. As we mentioned above, all the elements in the first column of the Yukawa coupling matrix are zero i.e.  $y_\Sigma^{\alpha 1} = 0$  for all values of  $\alpha$ . This implies  $\Sigma_1$  does not have Yukawa coupling with the SM lepton and Higgs. Thus, the neutral component of  $\Sigma_1$ ,  $\Sigma_1^0$  can be a suitable DM candidate.

### 3 Type III Seesaw explaining neutrino mass

As discussed in Section 2, among the three triplet fermions, the  $\mathbb{Z}_2$  odd one contributes to the DM phenomenology and the other two heavier generations take part in neutrino mass generation by the Type III seesaw mechanism. After the electroweak symmetry breaking, the neutrino mass matrix in the  $(\nu_L \ \Sigma_R^c)$  basis takes the following form,

$$\mathcal{L}_{NM} = -\frac{1}{2} (\overline{\nu_L} \ \overline{\Sigma_R^c}) \begin{pmatrix} 0 & M_D \\ M_D^T & M_\Sigma \end{pmatrix} \begin{pmatrix} \nu_R^c \\ \Sigma_R \end{pmatrix} + h.c. \quad (3.1)$$



It is evident that the mass matrix, written in  $(\nu_L \ \Sigma_R^c)$  basis, is a six dimensional square matrix if we consider three generations of light active neutrinos and three generations of fermion triplet. The constituent matrices  $M_D, M_\Sigma$  are square matrices of order  $3 \times 3$ . In contrast to the usual type-I seesaw mechanism, the first column of  $M_D$  is null since the Yukawa coupling of  $\Sigma_1$  is forbidden by the  $\mathbb{Z}_2$  symmetry. The three dimensional bare mass matrix of the triplet has been assumed to be diagonal with a hierarchical mass spectrum  $M_{\Sigma_1} \ll M_{\Sigma_2} < M_{\Sigma_3}$ . With the seesaw assumption i.e,  $M_\Sigma \gg M_D$ , we block diagonalize the mass matrix shown in Eq. (3.1), and get the following two eigenvalues (matrices) as,

$$\begin{aligned} m_\nu &\simeq -M_D M_\Sigma^{-1} M_D^T \\ M_\Sigma &\simeq \text{diag}(M_{\Sigma_1}, M_{\Sigma_2}, M_{\Sigma_3}). \end{aligned} \quad (3.2)$$

In Eq. (3.2),  $m_\nu$  is the active neutrino mass matrix and  $M_\Sigma$  is the heavy fermion triplet mass matrix. The effective neutrino mass matrix  $m_\nu$  has to be diagonalized further in order to get the light neutrino mass eigenvalues and mixing angles. In the present work, we are not concerned about the exact flavour structure of the neutrino mass matrix and thus we are not going into the details of the diagonalization procedure. Existing studies on Type-III seesaw leptogenesis have introduced a lower bound on the next to lightest triplet mass from BAU bound,  $M_{\Sigma_2} \gtrsim 3 \times 10^{10}$  GeV, which ensures sub-eV scale active neutrinos.

## 4 Lightest triplet as DM candidate

The lightest triplet  $\Sigma_1$  has been made stable by switching off its coupling to the SM particles through imposition of  $\mathbb{Z}_2$  discrete symmetry. The three components  $(\Sigma_1^+, \Sigma_1^0, \Sigma_1^-)$  of the triplet are degenerate at the tree level. However, the degeneracy is lifted when we consider radiative corrections [73]. In that case, the charged component becomes slightly heavier than the neutral one which makes the decay channel  $\Sigma_1^\pm \rightarrow \Sigma_1^0 + W^\pm(\text{virtual})$ <sup>4</sup> allowed. Thus  $\Sigma_1^0$  is the lightest stable particle in our particle spectrum, which has the potential to serve as a viable dark matter candidate by reproducing the correct relic abundance as predicted by the Planck collaboration [6].

### 4.1 Constraints on triplet DM

The detailed bound on the triplet fermion DM has been addressed in Ref. [74]. Considering the neutral component of the triplet fermion as WIMP DM candidate, the bound can come from direct detection, indirect detection and collider searches. In the present model, the WIMP-nucleon scattering cross-section occurs at one loop level and gets suppressed accordingly [73]. As a result, the spin independent scattering cross-section ( $\sigma_{\text{SI}}$ ) lies at least one order of magnitude below the present bound from LUX-ZEPLIN (LZ) [75] for  $M_{\Sigma_1} = 1$  TeV [37]. Moreover, a further suppression on  $\sigma_{\text{SI}}$  can arise due to the negative contribution of two loop gluon mediated processes [76]. On the other hand, in the present model, our DM candidate ( $\Sigma_1^0$ ) can only annihilate into  $W^+W^-$  final state at the tree level<sup>5</sup>. These  $W^\pm$  bosons eventually produce  $\gamma$ -rays after undergoing cascade processes involving pions. Accordingly, we have an existing bound on the  $\langle \sigma v \rangle_{W^+W^-}$  from gamma-ray telescopes like Fermi-LAT which is sensitive to  $\gamma$ -rays in the range  $\sim 20$  MeV to 300 GeV [72]. The recent bound on

<sup>4</sup>These virtual  $W^\pm$  decay into pions or leptons

<sup>5</sup>Coannihilations with charged partners,  $\Sigma_1^\pm$  are not considered here as these are not relevant for DM indirect detection.



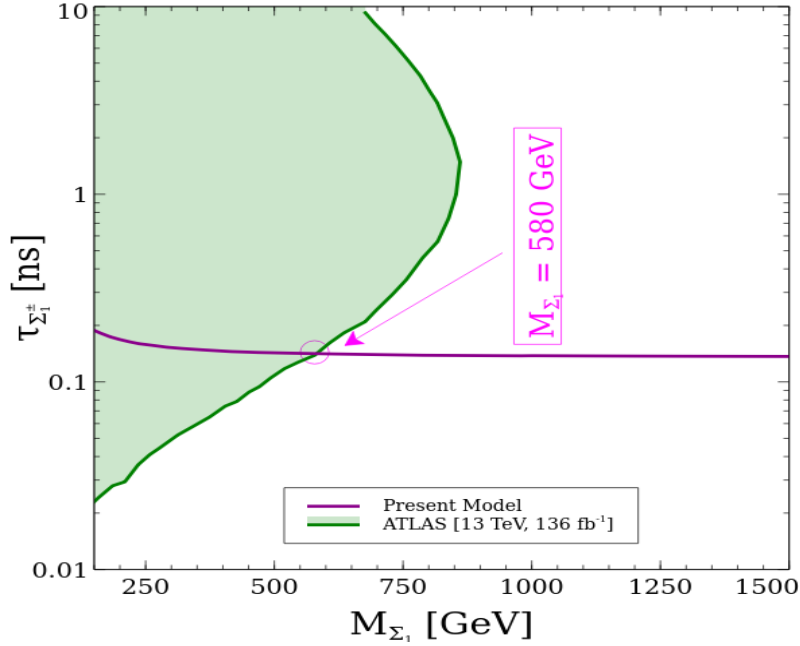


**Figure 1.** Collider bound on the mass of the triplet fermion when the neutral component is a DM candidate.

$\langle\sigma v\rangle_{W+W-}$  by Fermi-LAT through observation of  $\gamma$ -rays coming from dwarf spheroidal galaxies (dSph) [77] allows a narrow region of triplet DM mass between  $1000 \text{ GeV} \leq M_{\Sigma_1} \lesssim 1500 \text{ GeV}$ . For  $1500 \text{ GeV} \lesssim M_{\Sigma_1} \lesssim 2700 \text{ GeV}$ , there is a rapid growth in  $\langle\sigma v\rangle_{W+W-}$  due to the Sommerfeld enhancement [35, 36] and thus is ruled out from non-observation of excess gamma flux over the known astrophysical background. However, there is a more recent analysis in Ref. [78] where<sup>6</sup> the authors have derived a model independent bound on the total annihilation cross-section of dark matter after taking into account the bounds from Planck, Fermi-LAT and AMS.

The bound on  $M_{\Sigma_1}$  from collider searches has a similar search strategy as the SUSY charginos. As the mass difference between charged and neutral components,  $\Delta M = M_{\Sigma_1^\pm} - M_{\Sigma_1} \simeq 166 \text{ MeV}$  [73], is greater than the mass of charged pion,  $\Sigma_1^\pm$  decays predominantly into  $\Sigma_1^0$  and  $\pi^\pm$  with approximately 98% branching ratio. Due to the small mass gap  $\Delta M$ , the produced pion leaves a very short track at the collider. This kind of missing track searches put an upper bound on the triplet fermion mass and the current bound is  $M_{\Sigma_1} > 580 \text{ GeV}$  from ATLAS data with a luminosity of  $136 \text{ fb}^{-1}$  [79] (as shown in Fig. (1)). Moreover, there is a future projection of HL-LHC from  $3 \text{ ab}^{-1}$  luminosity data which will probe the triplet fermion mass up to  $870 \text{ GeV}$  [80]. In this context it should be mentioned that considering the bound given in Ref. [78], the lower bound on the triplet DM mass shifts to  $M_{\Sigma_1} \gtrsim 350 \text{ GeV}$  and in that case the bound from the LHC will be important. Most importantly, the collider bound is hard to evade with the introduction of beyond SM physics for the present setup, but we can easily evade the indirect detection bound by introducing an additional dark

<sup>6</sup>In the said reference the authors have argued that DM in the mass range  $20 - 10^5 \text{ GeV}$  is fully safe from the indirect detection searches (when DM particle under consideration is produced by the thermal freeze-out mechanism.). Here, we mention this result just as a general observation. However, it has not been used in our analysis.

annihilation channel of DM. For example, we can introduce a dark abelian gauge group under which  $\Sigma_1$  is charged and then DM can annihilate into dark gauge bosons and lower the indirect detection bound. Of course, in this kind of setup, we also need to take into account the gauge anomaly which can be addressed by introducing additional triplet fermion. The additional fermion mass can be kept beyond the inflation scale which will isolate its participation in our analysis. On the other hand, we can choose its mass at the lower scale which will have an impact on our DM analysis. Quantitatively, we anticipate that this kind of addition to our setup will change our DM phenomenology minimally but qualitatively there will be no change in our conclusion. This is just an example in the context of the present work to evade the indirect detection bound if the present model is in conflict with the future measurement of  $\gamma$ -ray data. It is to be mentioned that we have not implemented this type of extension in our present study and it is left for future exploration. Moreover, our leptogenesis study will remain unaffected because the triplet fermions which take part in leptogenesis are neutral under the dark abelian gauge group. For the lower mass range of DM, we have considered the collider bound on the DM mass to be stricter than the indirect detection bound, since the indirect detection bound can be evaded following the techniques discussed above. On the other hand for the higher mass range of DM, the indirect detection bound is more effective (or in other words hard to evade) due to the occurrence of the Sommerfeld enhancement peaks.

## 4.2 Evolution of comoving number density in non-standard cosmology

As discussed earlier the neutral component of the lightest triplet fermion,  $\Sigma_1^0$ , can be a very good DM candidate when we consider the corresponding Yukawa couplings are absent due to the imposition of  $\mathbb{Z}_2$  symmetry. Corresponding Boltzmann equation governing the evolution of DM comoving number density (a ratio of number density over entropy density  $s$ ) is given by,

$$\frac{dY}{dz} = -\frac{M_{\Sigma_1}}{z^2} \frac{1}{3H(T)} \frac{ds}{dT} \langle \sigma v \rangle_{\text{eff}} (Y^2 - Y_{eq}^2), \quad (4.1)$$

where  $z = \frac{M_{\Sigma_1}}{T}$  is a dimensionless quantity and  $s(T) = g_s(T) \frac{2\pi^2}{45} T^3$  with  $g_s(T)$  being the effective degrees of freedom (*d.o.f*) related to the entropy density  $s$ . The comoving density can also be expressed as  $Y = \sum_i Y_i$  where  $i$  runs for all the species in the dark sector i.e.,  $\Sigma_1^0$ ,  $\Sigma_1^+$  and  $\Sigma_1^-$ . The thermal averaged effective annihilation cross-section (denoted as  $\langle \sigma v \rangle_{\text{eff}}$ ) includes contributions from annihilation as well as co-annihilations involving dark sector species. The general expression of  $\langle \sigma v \rangle_{\text{eff}}$  is given by [81]

$$\begin{aligned} \langle \sigma v \rangle_{\text{eff}} &= \sum_{ij} \langle \sigma v \rangle_{ij} \frac{n_{\Sigma_1^i}^{eq} n_{\Sigma_1^j}^{eq}}{n_{\Sigma_1}^{eq} n_{\Sigma_1}^{eq}}, \\ &= \sum_{ij} \langle \sigma v \rangle_{ij} \frac{g_i g_j}{g_{\text{eff}}^2} (1 + \Delta_i)^{3/2} (1 + \Delta_j)^{3/2} \exp[-x(\Delta_i + \Delta_j)], \end{aligned} \quad (4.2)$$

where,  $n_{\Sigma_1^i}^{eq}$  is the equilibrium number density of the species  $i$  and thus the total equilibrium number density is given by  $n_{\Sigma_1}^{eq} = \sum_i n_{\Sigma_1^i}^{eq}$ . The last step of the above equation can be easily computed using the Maxwell-Boltzmann distribution with  $g_i$  being the internal degrees of freedom of species  $i$  and  $\Delta_i = (M_{\Sigma_1^i} - M_{\Sigma_1})/M_{\Sigma_1}$  is the fractional mass difference between

the species  $i$  and the lightest one which is nothing but our DM candidate  $\Sigma_1^0$ . Therefore,  $\Delta_i = 0$  and  $\Delta M/M_{\Sigma_1}$  for  $i = \Sigma_1^0$  and  $\Sigma_1^\pm$  respectively where  $\Delta M = M_{\Sigma_1^\pm} - M_{\Sigma_1} \simeq 166$  MeV as mentioned earlier. The quantity  $g_{\text{eff}}$  in the denominator is given by

$$g_{\text{eff}} = \sum_i g_i (1 + \Delta_i)^{3/2} \exp(-x\Delta_i). \quad (4.3)$$

The thermal averaged cross-section when the species  $i$  and  $j$  are in the initial state is denoted by  $\langle\sigma v\rangle_{ij}$ , where  $i = j = \Sigma_1^0$  represents DM annihilation while all other channels are co-annihilations. In the model under consideration, DM can only annihilate into  $W^+W^-$  final state. On the other hand, there are several co-annihilation channels like  $\Sigma_1^0 \Sigma_1^\pm \rightarrow W^\pm Z$ ,  $\Sigma_1^+ \Sigma_1^- \rightarrow W^+W^-$ ,  $\Sigma_1^+ \Sigma_1^- \rightarrow f\bar{f}$  ( $f$  is the SM fermion),  $\Sigma_1^\pm \Sigma_1^\pm \rightarrow W^\pm W^\pm$  and  $\Sigma_1^\pm \Sigma_1^\mp \rightarrow W^\pm W^\mp$ . These co-annihilation channels have a great impact on the freeze-out dynamics of DM as the mass gap between DM ( $\Sigma_1^0$ ) and the next-to-lightest species ( $\Sigma_1^\pm$ ) is around 166 MeV only, which is less than 0.02% of  $M_{\Sigma_1} = 1$  TeV. The expressions of individual annihilation and co-annihilation cross-sections along with  $\langle\sigma v\rangle_{\text{eff}}$  in  $s$ -wave approximation are given in Appendix A.

In the Boltzmann equation,  $H(T)$  is the Hubble parameter which depends on the total energy content of the Universe. However, due to the unavailability of experimental data before the BBN, the energy content of the Universe in that epoch is not well known to us. In this work, we will exploit this freedom by modifying the Hubble parameter before the BBN [48]. In particular, we consider an extra species  $\phi$  that increases the total energy density ( $\rho$ ) of the Universe by contributing dominantly before the BBN and  $\phi$  red-shifts faster than the radiation. As  $\rho > \rho_{\text{rad}}$ , the Hubble parameter is also large compared to the standard case of the radiation domination and thus the scenario is referred to as the fast expanding Universe in the literature [48]. The expansion rate of the Universe is quantified by the Hubble parameter which is related to the total energy density of the Universe as,

$$H(T) = \sqrt{\frac{8\pi G \rho(T)}{3}}, \quad (4.4)$$

where  $G$  is the Gravitational constant. The total energy density is now the sum of two components, i.e.,

$$\rho(T) = \rho_{\text{rad}}(T) + \rho_\phi(T). \quad (4.5)$$

The first term ( $\rho_{\text{rad}}$ ) is the radiation contribution to the energy density, which dominates the total energy budget in the standard cosmology before the era of matter-radiation equality ( $T \simeq 0.8$  eV) and has the following form,

$$\rho_{\text{rad}}(T) = \frac{\pi^2}{30} g_*(T) T^4, \quad (4.6)$$

where,  $g_*(T)$  is the effective relativistic *d.o.f* related to the radiation energy density at the concerned temperature. On the other hand, the second term in Eq. (4.5), representing energy density of the species  $\phi$ , red-shifts as [48],

$$\rho_\phi \propto a^{-(4+n)}, \quad (4.7)$$

with  $n > 0$ . Since  $\rho_\phi$  red-shifts faster ( $\rho_\phi \propto T^{4+n}$  as  $a \propto T^{-1}$ ) than the radiation, we can have a Universe dominated by the energy density of  $\phi$  in the pre-BBN era and reduces to the standard picture at  $T \leq T_r$ . Imposing the entropy conservation in a unit co-moving volume, the energy density  $\rho_\phi$  takes the following form [48],

$$\rho_\phi(T) = \rho_\phi(T_r) \left( \frac{g_s(T)}{g_s(T_r)} \right)^{\frac{4+n}{3}} \left( \frac{T}{T_r} \right)^{4+n}, \quad (4.8)$$

where, the reference temperature  $T_r$  is defined as the temperature where contributions of the radiation and the species  $\phi$  becomes equal and for  $T < T_r$  we have the usual radiation dominance. Finally, using Eqs. (4.6 and 4.8), the total energy density at any temperature can be written as

$$\begin{aligned} \rho(T) &= \rho_{\text{rad}}(T) + \rho_\phi(T) \\ &= \rho_{\text{rad}}(T) \left[ 1 + \frac{g_*(T_r)}{g_*(T)} \left( \frac{g_s(T)}{g_s(T_r)} \right)^{\frac{4+n}{3}} \left( \frac{T}{T_r} \right)^n \right], \\ &= \rho_{\text{rad}}(T) \left[ 1 + \left( \frac{g_*(T)}{g_*(T_r)} \right)^{\frac{1+n}{3}} \left( \frac{T}{T_r} \right)^n \right]. \end{aligned} \quad (4.9)$$

In the last step, we consider  $g_*(T) = g_s(T)$ , which is valid before the era of neutrino decoupling that takes place around  $T \sim 1$  MeV. Therefore, for  $T \gg T_r$ ,  $\rho(T) \gg \rho_{\text{rad}}(T)$  and thus the Hubble parameter gets enhanced according to Eq. (4.4), which has a great impact on the evolution of particles in the early Universe. In this work, we will study the impact of such non-standard cosmology on our DM candidate and also on the matter anti-matter asymmetry of the Universe in the context of a typical BSM model where the SM particle spectrum is extended by three additional  $\text{SU}(2)_L$  triplet fermions. As we mentioned earlier, this model potentially explains the three important issues of the SM, namely the nature of dark matter, the origin of tiny neutrino mass and the physics behind the observed asymmetry between matter and anti-matter of the Universe.

#### 4.2.1 Determining the freeze-out temperature $T_f$

As discussed in the preceding section, the presence of an extra species in the early Universe modifies the Hubble parameter in the following manner,

$$H(T) = \sqrt{\frac{8\pi^3 G g_*(T)}{90}} T^2 \left[ 1 + \left( \frac{g_*(T)}{g_*(T_r)} \right)^{\frac{1+n}{3}} \left( \frac{T}{T_r} \right)^n \right]^{1/2}, \quad (4.10)$$

$$= H_{\text{rad}}(T) \left[ 1 + \left( \frac{g_*(T)}{g_*(T_r)} \right)^{\frac{1+n}{3}} \left( \frac{T}{T_r} \right)^n \right]^{1/2}. \quad (4.11)$$

In terms of  $z$  ( $= \frac{M_{\Sigma_1}}{T}$ ), the Hubble parameter is given by

$$H(z) = H_{\text{rad}}(z) f(z, z_r, n), \quad (4.12)$$

where, the function  $f(z, z_r, n)$  (following definition of  $z$ ,  $z_r = \frac{M_{\Sigma_1}}{T_r}$ ) is defined as

$$f(z, z_r, n) = \left[ 1 + \left( \frac{g_*(M_{\Sigma_1}/z)}{g_*(M_{\Sigma_1}/z_r)} \right)^{\frac{1+n}{3}} \left( \frac{z_r}{z} \right)^n \right]^{1/2}, \quad (4.13)$$

and  $H_{\text{rad}}$  is the Hubble parameter for the standard radiation dominated Universe. Since the reference temperature  $T_r \ll T_f$ , the function  $f(z, z_r, n)$  can be significantly larger than unity and this results in an enhanced Hubble parameter. The increase in the Hubble parameter will make the freeze-out of dark matter happen earlier in time. In the thermal WIMP paradigm, DM gets thermally decoupled from the cosmic fluid once the interaction rate of DM falls below the corresponding expansion rate of the Universe and we can determine the freeze-out temperature by solving the following equation,

$$H(T) = n_{\Sigma_1}^{eq} \langle \sigma v \rangle_{\text{eff}} \text{ at } T = T_f, \quad (4.14)$$

where,  $n_{\Sigma_1}^{eq}$  and  $\langle \sigma v \rangle_{\text{eff}}$  are already defined earlier in Sec. 4.2. Upon simplifying<sup>7</sup> the above equality using the expressions of Hubble parameter (Eq. (4.12)) in non-standard cosmology, the equilibrium number density of the DM particle and effective annihilation cross-section, we get the following transcendental equation for  $z_f$ ,

$$z_f \simeq 28 - \ln \left[ \frac{M_{\Sigma_1}}{1000 \text{ GeV}} \right] - \ln [f(z_f, z_r, n)] + \frac{1}{2} \ln [z_f], \quad (4.15)$$

which can be solved iteratively to obtain the freeze-out temperature  $T_f (= \frac{M_{\Sigma_1}}{z_f})$ . It is to be noted that Eq. (4.15) contains an additional term (with negative sign), compared to its standard counterpart, which depends on two non-standard parameters  $n, T_r$ . In our study, we have focused on the regime where the non-standard contribution is large, which implies a significant negative contribution due to the  $\ln [f(z_f, z_r, n)]$  term and hence,  $z_f$  in our case turns out to be much smaller than that of the standard radiation dominated case. The lower value of  $z_f$  clearly signifies that our DM candidate freezes out at a higher temperature. So we can expect a higher relic abundance than the standard cosmological scenario. It is worth mentioning here that in the standard scenario, we could have lowered the  $z_f$  value only by increasing the DM mass  $M_{\Sigma_1}$  (i.e. by reducing  $\langle \sigma v \rangle_{\text{eff}}$ ). However, the introduction of non-standard cosmology, where we have two additional parameters  $n, T_r$ , can result in a similar kind of lowering in  $z_f$ . We will see later in this study that the reduction in  $z_f$  due to the non-standard parameters will help us obtaining the correct value of relic density for the lower values of dark matter mass which is not at all possible in the standard case of radiation domination.

#### 4.2.2 Analytical approximation for DM relic density

We can solve the Boltzmann equation given in Eq. (4.1) analytically in the limit where effective degrees of freedom  $g_*$  is not changing significantly with temperature, which is valid as long as the freeze-out occurs well above the era of QCD phase transition ( $T \sim 100 \text{ MeV}$ ). The comoving number density after freeze-out ( $z > z_f$  or  $T < T_f$ ) can be obtained easily as

$$Y_{\Sigma_1}(z) \simeq \left[ \frac{1}{Y_{\Sigma_1}(z_f)} + \sqrt{\frac{\pi}{45}} M_{\Sigma_1} M_{pl} J(z, z_r, n) \right]^{-1}, \quad (4.16)$$

---

<sup>7</sup>This simplification can be found in appendix B ( Eq. (B.5) - Eq. (B.7) ).

where  $z = \frac{M_{\Sigma_1}}{T}$  as defined before, the function  $J(z, z_r, n)$  contains  $\langle \sigma v \rangle_{\text{eff}}$  and it also depends on the non-standard cosmology parameters in the following way

$$J(z, z_r, n) = \int_{z_f}^z \frac{g_*^{1/2} \beta(z') \langle \sigma v \rangle_{\text{eff}}}{f(z', z_r, n) z'^2} dz', \quad (4.17)$$

and

$$\beta(z') = 1 - \frac{1}{3} \frac{d \ln g_*(z')}{d \ln z'}.$$

Assuming  $g_*$  does not change vigorously over the region of integration (which also implies  $\beta \simeq 1$ ) and the enhancement factor  $f \gg 1$ , the above integration can be simplified as

$$J(z, z_r, n) \simeq \left( \frac{g_*(M_{\Sigma_1}/z_r)}{\bar{g}_*} \right)^{\frac{1+n}{6}} \sqrt{\frac{\bar{g}_*}{z_r^n}} \int_{z_f}^z \frac{\langle \sigma v \rangle_{\text{eff}}}{z'^{2-n/2}} dz'. \quad (4.18)$$

In the above expression for  $J$ , if we neglect the first term within the brackets and set  $z_r = 1$  and  $n = 0$ , we will recover the function  $J$  for the radiation dominated Universe. In the present model, we have  $s$  wave annihilations and the expression of  $\langle \sigma v \rangle_{\text{eff}}$  under  $s$  wave approximation is given in Appendix A. This allows us to compute the function  $J$  analytically as

$$J(z, z_r, n) \simeq \left( \frac{g_*(M_{\Sigma_1}/z_r)}{\bar{g}_*} \right)^{\frac{1+n}{6}} \sqrt{\frac{\bar{g}_*}{z_r^n}} \langle \sigma v \rangle_{\text{eff}} \times \begin{cases} \frac{2}{2-n} \left( \frac{1}{z_f^{1-n/2}} - \frac{1}{z^{1-n/2}} \right) & \text{for } n \neq 2 \\ \ln(z/z_f) & \text{for } n = 2 \end{cases} \quad (4.19)$$

The presence of  $z_r^{n/2}$  ( $z_r \gg 1$ ) in the denominator makes the function  $J$  suppressed compared to the case of radiation domination which eventually increases the comoving number density through Eq. (4.16) for a fixed value of  $\langle \sigma v \rangle_{\text{eff}}$ . The Eq. (4.18) matches with Ref. [48] except the factor within the brackets which the authors have considered  $\sim \mathcal{O}(1)$ . Finally, once we have the co-moving number density then we can determine the DM relic density using the following expression,

$$\Omega_{\text{DM}} h^2 = 2.755 \times 10^8 \left( \frac{M_{\Sigma_1}}{\text{GeV}} \right) Y_{\Sigma_1}(z \gg z_f). \quad (4.20)$$

### 4.2.3 BBN Bound

The extra species  $\phi$  can contribute adequately to the total energy density and hence to the Hubble parameter ( $H$ ) during the epoch of BBN depending on the parameters  $T_r$  and  $n$ . The extra energy<sup>8</sup> that can be accommodated at the time of BBN over the standard radiation background is estimated in terms of parameter  $N_{\text{eff}}$  as

$$\Delta \rho = \Delta N_{\text{eff}} \rho_{\nu_L}, \quad (4.21)$$

where,  $\rho_\nu = \frac{7}{8} \alpha_{\nu/\gamma} \rho_\gamma$  is the energy of a single species of active neutrino at BBN and  $\alpha_{\nu/\gamma} = \left( \frac{4}{11} \right)^{1/3}$  is the ratio of active neutrino to photon temperature after neutrino decoupling around  $T \lesssim 1$  MeV<sup>9</sup>. The allowed value of  $\Delta N_{\text{eff}}$  based on standard cosmological history around the BBN is given by [82]

$$\Delta N_{\text{eff}} = N_{\text{eff}}^{\text{BBN}} - N_{\text{SM}} = 0.374 \text{ at } 95\% \text{ C.L.}, \quad (4.22)$$

<sup>8</sup>The extra energy should be red-shifted at least equal to or faster than the radiation energy.

<sup>9</sup>In our numerical analysis, we consider  $\alpha_{\nu/\gamma} = 1$ .

where, theoretical prediction of  $N_{\text{eff}}$  based on the SM is  $N_{\text{eff}} = 3.046$  [83, 84] and  $N_{\text{eff}}^{\text{BBN}} = 2.88 \pm 0.27$  at 68% C.L. [82]. Now, assuming the extra contribution from  $\phi$  remains within the allowed limit gives the lower limit of the transition temperature  $T_r$  for a particular value of index  $n$

$$T_r \geq \left( \frac{g_s(T_{\text{BBN}})}{g_s(T_r)} \right)^{\frac{4+n}{3n}} \left( \frac{g_s(T_r)}{0.65 \alpha_{\nu/\gamma}^4} \right)^{1/n} \text{ MeV}. \quad (4.23)$$

The above bound has been used in all the scatter plots and in particular a sharp effect of this bound can be observed in the  $n - T_r$  plane of RP of Fig. (7) and LP of Fig. (10).

### 4.3 Numerical results: viability of fermion triplet DM

In this section, we are going to discuss the numerical findings of our study with special emphasis on evolution of DM relic density in non-standard cosmological background. We will proceed through graphical representation of numerical results followed by meticulous analysis of those figures in order to realize the impact of non-standard cosmology towards generation of adequate relic abundance.

Various line plots systematically analyze the possibility of earlier freeze-out of the DM in the modified cosmological scenario. The extent of non-standard contribution is quantified by the parameters  $T_r, n$  which play a pivotal role in modifying evolution of the DM relic abundance and thus the frozen value of the relic density can be altered significantly by tuning the said non-standard parameters. Larger relic abundance (compared to the standard case), in agreement with the current experimental data, can be obtained for a lower mass, of the dark matter, which is allowed by the indirect detection bound as well as the bound obtained from collider searches. This entire phenomenon has been depicted through numerous line plots in Sec. 4.3.1.

Relic density depends on the model parameters  $(M_{\Sigma_1}, T_r, n)$  in a bit complicated manner. To understand the nature of this dependence, when the parameters are varied simultaneously, we show scatter plots of frozen value of the relic density with mass of the triplet DM, where the non-standard parameters are shown by colour variation. Limiting values of these parameters  $(M_{\Sigma_1}, T_r, n)$ , required for successful prediction of DM relic density, have been estimated from similar scatter plots presented in the following Sec. 4.3.1.

#### 4.3.1 Graphical analysis of numerical results

In the left panel (LP) of Fig. (2), we have shown variation in  $z - \frac{n_{eq} \langle \sigma v \rangle_{\text{eff}}}{H(T)}$  plane where  $n_{eq} = \frac{g_{\Sigma} M_{\Sigma}^3 K_2(z)}{2\pi^2 z}$ . Here  $K_2(z)$  is the modified Bessel function of second kind,  $H(T)$  is Hubble parameter at temperature  $T$  (defined in Eq. (4.4)) and  $\langle \sigma v \rangle_{\text{eff}}$  is the effective annihilation cross-section (defined in Eq. (A.2)). It is to be noted that the proposed DM candidate gets decoupled from the thermal plasma as soon as the corresponding reaction rate becomes less than the Hubble parameter at that instant. In the above figure, we have plotted the ratio of these two quantities, the out of equilibrium condition is satisfied whenever the value of this ratio falls below unity. Thus it is clear from the figure (LP) that, as we increase the value of  $n$ , the DM goes out of equilibrium for a lower value of  $z$  (or equivalently for a higher value of temperature  $T$ ). In other words, the DM freezes earlier for higher values of  $n$ . Hence it can be inferred that with the increment of non-standard contribution, our DM goes out of



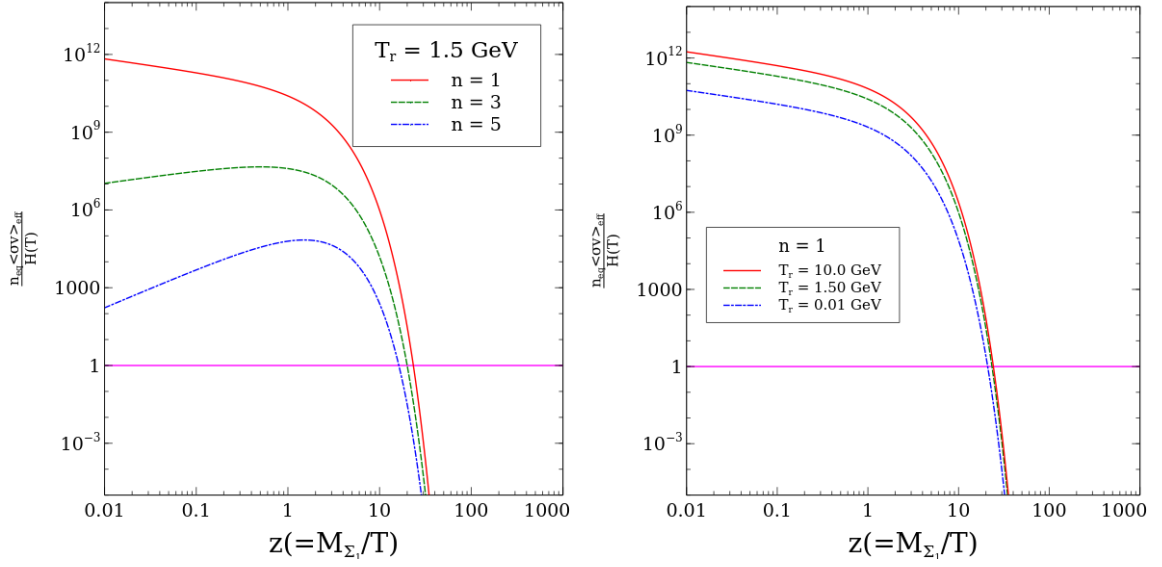


**Figure 2.** LP and RP show the out of equilibrium check of DM for three different values  $n$  and  $T_r$ , respectively.

equilibrium earlier and thus we will get higher DM abundance (as obtained from Eq. (4.15)). On the other hand in the right panel (RP), we have shown variation of the same quantity (as in LP) for three different values of  $T_r$  while  $n$  is kept fixed. From the figure (RP), it is clear that lowering the value of  $T_r$  causes earlier freeze-out, which implies a greater relic abundance of the DM.

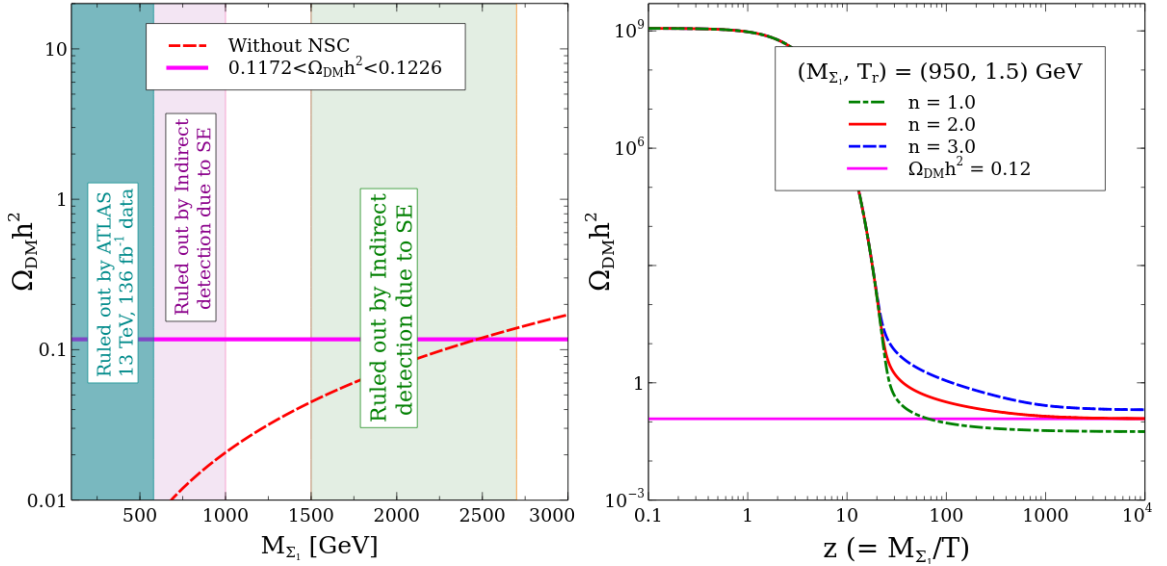


**Figure 3.** LP: Variation of DM relic density with the DM mass for standard cosmology (red dashed line) and non-standard cosmology (green solid line). RP: Variation of DM relic density with  $z$  for three different values of  $n$ .

In the LP and RP of Fig.(3), we have shown line plots in the  $M_{\Sigma_1} - \Omega_{DM} h^2$  and  $z - \Omega_{DM} h^2$  planes, respectively. In the LP, we have shown the dependence of relic density

on DM mass where the red dashed line corresponds to the pure triplet model with standard cosmology<sup>10</sup> and the green solid line represents the case with non-standard cosmological background before the BBN. The green region is ruled out by Fermi-LAT due to the presence of the Sommerfeld enhancement spike around that specific mass range. The magenta region is also ruled excluded by Fermi-LAT and the cyan region is ruled out by the missing track search at the LHC. From the figure, it is clear that we have a very narrow window between 1000–1500 GeV which is allowed after considering all the existing bounds mainly the indirect detection bound. As discussed in Section 4.1, the indirect detection bound can be evaded by introducing an additional annihilation mode of DM. Therefore from the lower mass end, the collider bound ( $M_{\Sigma_1} > 580$  GeV) can be regarded as stricter than the indirect detection bound, whereas it is difficult to escape the indirect detection bound between 1.5 TeV and 2.7 TeV due to the presence of a spike (coming from the Sommerfeld enhancement factor) in the annihilation cross-section around the above mentioned mass range. We can see that without non-standard cosmology it is very difficult to satisfy the DM relic density in the correct ballpark value. On the other hand, if we introduce non-standard cosmology before BBN then it helps to decouple the DM from the thermal bath earlier (can be seen from Eq. (4.15)) and hence the higher value of relic abundance can be obtained. Therefore, we can clearly see that for  $n = 2$  and  $T_r = 1.5$  GeV, we can easily satisfy DM relic density for mass  $M_{\Sigma_1} = 950$  GeV. On the other hand, in the RP, we have shown the DM relic density variation with  $z$  for three different values of  $n$ . It is clear from the said figure that as we increase the value of  $n$ , the DM relic abundance is also enhanced. This is in agreement with the conclusion obtained from Fig. (2). The most important information obtained from Fig. (3) is, in the non-standard scenario we can get the correct value of DM relic density for DM mass  $M_{\Sigma_1} = 950$  GeV which is not achievable for the same DM mass within the framework of standard cosmology.

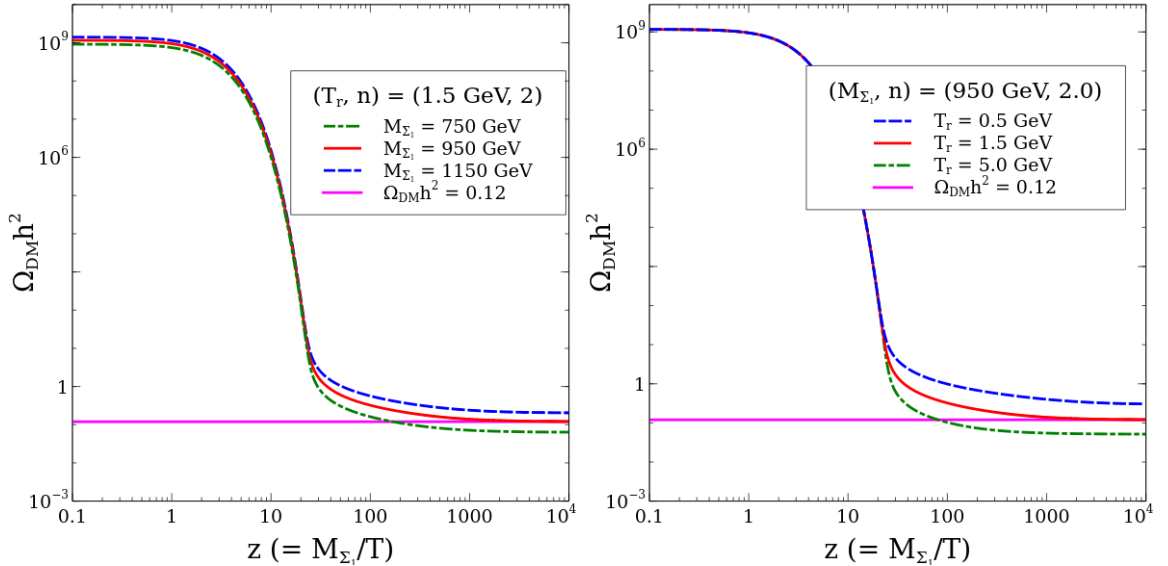


**Figure 4.** LP and RP show the evolution of DM relic density with  $z$  for three different values of DM mass  $M_{DM}$  and reference temperature  $T_r$ , respectively.

In the LP and RP of Fig. (4), we have shown the variation of DM relic density with  $z$

<sup>10</sup>The line will be a little lower if we include the Sommerfeld factor in the relic density calculation and the correct value of DM relic density can be obtained for  $2.7 \lesssim M_{\Sigma_1}$  (TeV)  $\lesssim 3$  [85].

for three different values of DM mass  $M_{\Sigma_1}$  (while  $T_r, n$  kept fixed) and  $T_r$  (while  $M_{\Sigma_1}, n$  kept fixed), respectively. It can be seen from the LP of the figure that increment of DM mass enhances its relic density. This can be clearly understood from Eq. (A.1) that thermal average cross-sections are inversely proportional to the square of the DM mass and the relic density is inversely proportional to the thermal average cross-sections (Eq. (4.16)). Therefore the DM relic density behaviour with mass is justified. The red solid line signifies that correct value of DM relic density can be obtained for  $M_{\Sigma_1} = 950$  GeV while the non-standard parameters are kept at a value  $T_r = 1.5$  GeV and  $n = 2$ . On the other hand, in the RP, we have shown the DM relic density variation for three different values of  $T_r$ . We have already discussed in the context of Fig. (2) that smaller values of  $T_r$  implies more non-standard contribution in the DM production. The same behaviour of relic density is reflected in the RP of Fig. (4), i.e if we lower the value of  $T_r$ , we will have more non-standard contribution in DM relic density and vice versa. The  $T_r$  and  $n$  dependence of DM production will be more vivid when we discuss the scatter plots among the different parameters in the forthcoming figures.

In this part, we are going to show a few scatter plots among the model parameters which affect the DM relic density significantly. The relevant parameters are  $M_{\Sigma_1}$ ,  $n$  and  $T_r$  which have been varied in the following range (keeping in mind the upper bound on DM mass and BBN bound on  $T_r$ ),

$$500 \text{ GeV} \leq M_{\Sigma_1} \leq 1500 \text{ GeV}, 10^{-4} \leq n \leq 5, \text{ and } 10^{-3} \text{ GeV} \leq T_r \leq 10^3 \text{ GeV}. \quad (4.24)$$

In the LP of Fig. (5), we have shown scatter plot in the  $M_{\Sigma_1} - \Omega_{\text{DM}} h^2$  plane allowing only

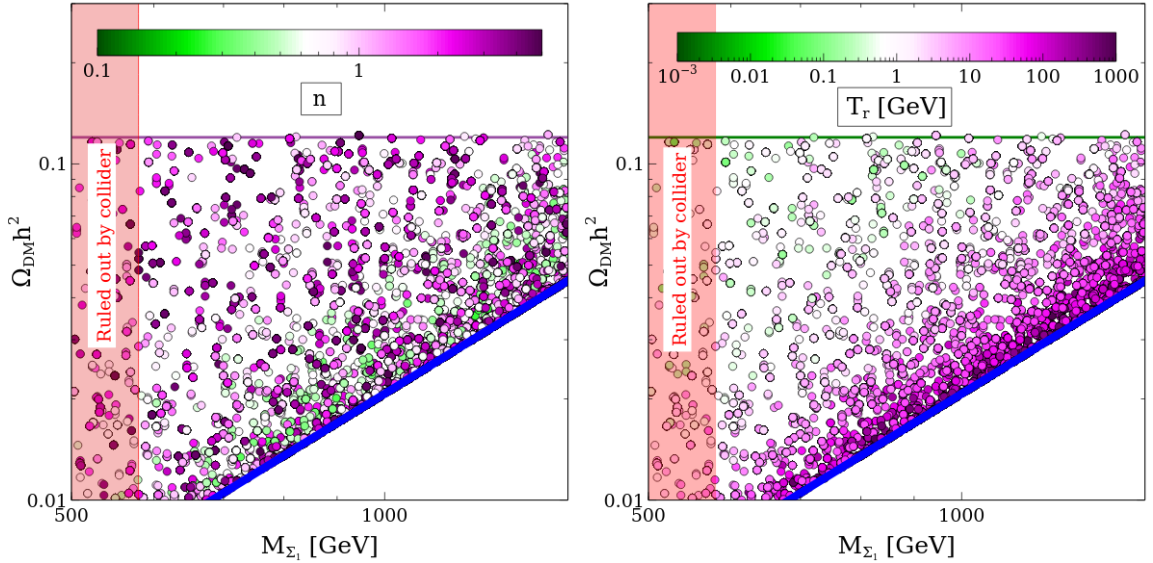


**Figure 5.** LP: Scatter plot in the  $M_{\Sigma_1} - \Omega_{\text{DM}} h^2$  plane with the colour variation in the parameter  $n$ . In the RP, the same scatter plot but the color variation represent the parameter  $T_r$ . In both panels, the DM relic density has been assumed in the range 0.01 to 0.12.

those points for which relic density lies within the range of 0.01 – 0.12. Moreover, It should be noted that in the scatter plots we have chosen strictly those combinations of  $(T_r, n)$  which respect the BBN bound given in Eq. (4.23). Basically, the plots of LP and RP (in Fig. 5) both represent exactly the identical data-set composed of  $(T_r, n, M_{\Sigma_1}, \Omega_{\text{DM}} h^2)$ . In LP variation of

$n$  is shown by colour bar whereas in RP same technique is used to designate  $T_r$ . The pink shaded<sup>11</sup> region is already ruled out by the  $136 \text{ fb}^{-1}$  luminosity data of LHC. The blue solid line (in LP as well as RP of Fig. (5)) corresponds to the DM relic density variation with DM mass without any non-standard contribution. The  $n$  value of any particular point in the plot can be retrieved from its colour. The horizontal colour bar shows continuous variation of  $n$  with colour. Before explaining this figure if we look at Eq. (4.9), we see that for  $n > 1$  we can have a sizeable contribution, from the non-standard part, comparable to the standard part. On the other hand, if we take  $T_r \gg 1$  the non-standard contribution, to the DM evolution, can be reduced to a large extent. In the figure, the lower sharp line (coinciding with the blue line) corresponds to the DM relic density for corresponding DM masses when non-standard contribution is negligible *i.e.*

$$\lim_{n>1, T_r \gg 1} \left( \frac{g_*(T)}{g_*(T_r)} \right)^{\frac{1+n}{3}} \left( \frac{T}{T_r} \right)^n \ll 1.$$

It can also be seen from the figure that the green points correspond to  $n < 1$  which gives more contribution than the standard contribution because of less suppression due to the aforementioned effect. But as we have seen in Fig. (2), the larger values of  $n$  imply more contribution from the non-standard cosmology and this is also consistent with the present figure because if we take a fixed value of  $M_\Sigma$  and move along the ordinate then the DM relic density increases with the increase of  $n$ . In the RP of the same figure we have used similar kind of colour variation to bring out the nature  $T_r$  dependence of relic density. The dark-pink points, represent higher values of  $T_r$ , give a smaller contribution in DM relic density which is reflected in the region of negligible non-standard contribution. In the RP, for a fixed value of  $M_\Sigma$ , if we move along the y coordinate we get an increment in DM relic density which corresponds to lower values of  $T_r$  as represented by the colour variation. In both the figures, It has been checked explicitly that, for  $n < 0.4$  we can never achieve the correct value of DM relic density for the allowed DM mass range. We can't go below  $n = 0.4$  since it would result in a large value of  $T_r$  (obtained from the bound of Eq. (4.23)) which again tends to nullify the non-standard effect.

In the LP of Fig. (6), we have shown the scatter plot in  $M_{\Sigma_1} - n$  plane where the colour bar corresponds to the DM relic density in the range  $0.05 - 0.12$  and like Fig. (5), we have also demanded that all the points satisfy BBN bound represented by Eq. (4.23). We know from the LP of Fig. (3) that without non-standard cosmology  $M_{\Sigma_1} = 1200 \text{ GeV}$  corresponds to DM relic density  $\Omega_{\text{DM}} h^2 \sim 0.03$ . Thus from Fig. (6), it is clear that if the DM mass is in the range of  $500 - 1200 \text{ GeV}$  and the non-standard parameter in the range  $0.1 \leq n \leq 0.4$ , we can not have DM relic density around  $0.05$  for the whole range of  $T_r$  considered in our work and therefore this region is not allowed. The correct value of DM relic density can be achieved for the whole range of DM mass if we are in the region  $n > 1$  whereas the value of  $n$  can be as low as  $\sim 0.4$  if we take  $M_{\Sigma_1} \sim 1500 \text{ GeV}$ . For the range  $1200 < M_{\Sigma_1} (\text{GeV}) < 1500$  and  $0.1 < n < 0.4$ , the non-standard is not sufficient to produce the correct value of DM relic density. On the other hand in the RP we have shown the variation of the parameters  $M_\Sigma - T_r$  which produce DM relic density in the range of  $0.05 - 0.12$ . It can be noticed from the figure that for the range  $10 < T_r (\text{GeV}) < 1000$  and  $500 < M_{\Sigma_1} (\text{GeV}) < 1200$ , the non-standard contribution is not sufficient to raise the DM relic density up to  $\Omega_{\text{DM}} h^2 = 0.05$ . On the other hand, if we take  $T_r$  below  $10 \text{ GeV}$ , we can always obtain the correct value of

<sup>11</sup>The pink shaded regions in the other plots imply the same thing.

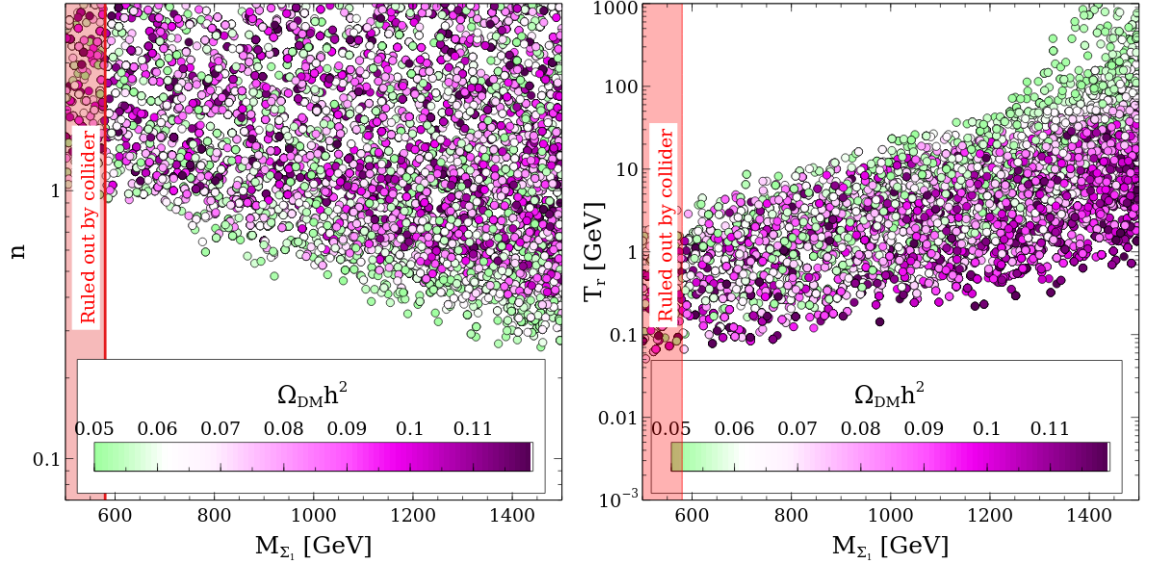


**Figure 6.** LP and RP show the scatter plots in the  $M_{\Sigma_1} - n$  and  $M_{\Sigma_1} - T_r$  plane after demanding DM relic density in the range 0.05 to 0.12. In both the panel the color variation shows the variation of DM relic density.

DM relic density. For the range  $10 < T_r(\text{GeV}) < 1000$  and  $1200 < M_{\Sigma_1}(\text{GeV}) < 1500$ , the non-standard contribution is not sufficient to have the correct value of DM relic density.

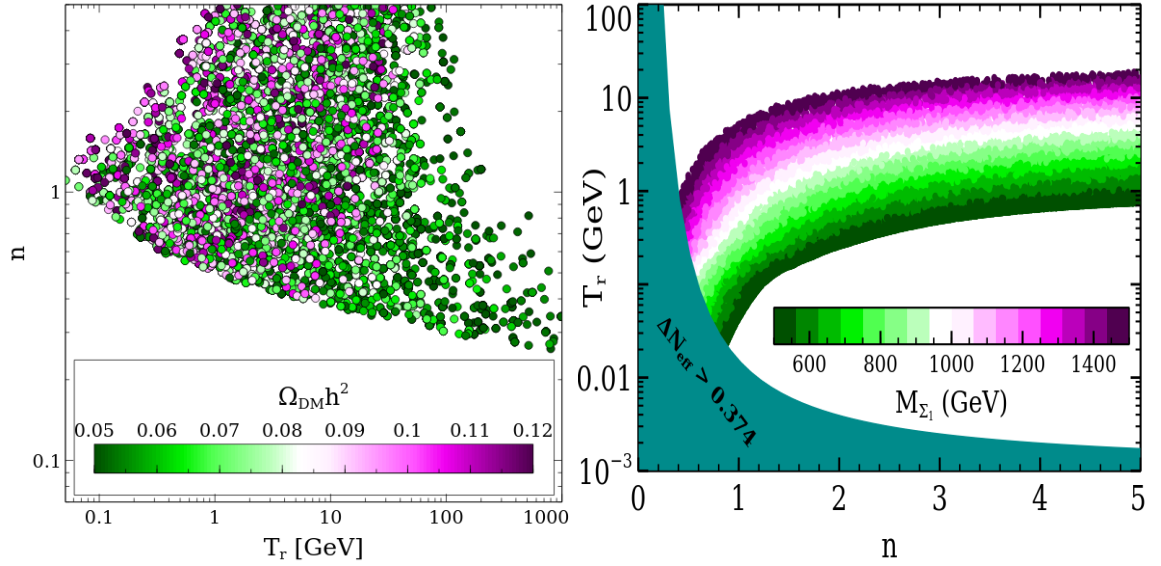


**Figure 7.** Scatter plot in the  $T_r - n$  plane after demanding DM relic density in the 0.05 – 0.12. The colour variation represents DM relic density.

In the LP of Fig. (7), we have shown variation in the  $T_r - n$  plane upon imposing the constraint that DM relic density (which is depicted in the colour bar) should lie within the range 0.05 – 0.12. The top-left corner region represents an overabundant region, i.e. the DM relic density  $\Omega_{DM} h^2 > 0.12$ . This can be easily understood since the region corresponds to



a large non-standard contribution which drives the relic abundance towards a higher value. On the contrary, we do not have any points in the top-right corner because that region has less contribution from non-standard cosmology due to the high value of  $T_r$ . Thus our DM is severely underabundant in that region ( $\Omega_{\text{DM}} h^2 < 0.05$ ). We also have discussed before that we can never get the correct value of relic density ( $0.117 \leq \Omega_{\text{DM}} h^2 \leq 0.123$ ) for  $M_{\Sigma_1} \leq 1.5$  TeV if we are below  $n = 0.4$ . This figure also confirms the fact that the region below  $T_r \lesssim 10$  GeV and  $n > 0.4$  can reproduce the correct value of DM relic density. In the RP, we have shown the allowed region in  $n - T_r$  plane that satisfies DM relic density in the  $3\sigma$  range only. While doing this scanning, we have varied all three variables  $n$ ,  $T_r$  and  $M_{\Sigma_1}$  simultaneously. The corresponding variation of DM mass has been indicated by the colour bar in the range  $500 \text{ GeV} \leq M_{\Sigma_1} \leq 1500 \text{ GeV}$ . The region disallowed by BBN for producing excess  $\Delta N_{\text{eff}}$  (as given in Eq. (4.23)) is shown by the dark cyan colour. From this plot, one can easily notice that a larger DM mass is required to satisfy  $\Omega_{\text{DM}} h^2$  in  $3\sigma$  range when the effect of non-standard cosmology is small i.e. for the lower values of  $n$  and the higher values of  $T_r$ . Similarly, as we increase the DM mass, the correct value of DM density can be achieved for a bit higher value of  $T_r$ . However, once we go beyond  $T_r \simeq 20$  GeV then one can never achieve the correct DM relic abundance for any value of  $n$  when  $M_{\Sigma_1} \leq 1.5$  TeV. In the later part of the article, we will further constrain the  $n - T_r$  parameter space once we impose the BAU bound.

## 5 Baryogenesis through Type-III seesaw leptogenesis

The popular Type-I seesaw [27–30] mechanism (SM + three generations of a gauge singlet heavy fermion), is primarily introduced to explain the non-zero mass of the active neutrinos, it has the potential to account for the observed baryon asymmetry of the Universe. Presence of Majorana type mass term in the Lagrangian ensures the lepton number violation by two units. The CP violating out of equilibrium decay of the singlet fermions (right handed neutrinos) to lepton Higgs pair gives rise to lepton asymmetry which gets converted into baryon asymmetry by sphaleron interactions [86].

If the said fermion singlet is replaced by  $\text{SU}(2)_L$  triplet fermion, the Majorana mass term and the Yukawa coupling term seems to be identical to that of the singlet except the fact that the Yukawa term now consists of three fold extra terms (which signifies the three components of the triplet) compared to its singlet counterpart. Unlike the singlets, the fermion triplets have gauge interactions. At high temperature these gauge interactions are strong enough to promptly drive the triplet abundance to its equilibrium value. Thus in this case the final asymmetry is almost independent of the initial condition (i.e. whether we start from vanishing /equilibrium initial abundance).

The preliminary objective of this work is to assess the viability of fermion triplet DM (which is very tightly constrained by indirect detection searches of DM and collider searches) in a non-standard cosmological background. The neutral component of the lightest triplet acts as a DM candidate since it is odd under  $\mathbb{Z}_2$  discrete symmetry, whereas the heavier generations of the triplet as well as the whole SM particle content are even under  $\mathbb{Z}_2$ . The next to lightest triplet, having normal Yukawa coupling can decay to lepton, Higgs pair to produce the CP asymmetry required to explain the BAU. Existing studies [68–70] in the literature dealing with hierarchical fermion triplet leptogenesis have already set a lower bound on the

mass of the lightest decaying triplet to be  $M_\Sigma \gtrsim 3 \times 10^{10}$  GeV<sup>12</sup>. It is to be noted that the said lower bound also depends on the effective neutrino mass parameter ( $\tilde{m}$ ) and its specific value mentioned above can be obtained for  $\tilde{m} \sim 0.001$  eV. It can be found from the concerned plot [68, 70] of allowed (by BAU bound) parameters in  $M_{\Sigma_2} - \tilde{m}$  plane, that the lowest allowed value of  $M_{\Sigma_2}$  lies near  $10^{11}$  GeV over a wide range of  $\tilde{m}$ . Thus in the remaining portion of our analysis  $10^{11}$  GeV is referred to as the lower limit of  $M_{\Sigma_2}$  for standard cosmology.

Now in context of non-standard cosmology, it will be an intriguing study to examine whether the above mentioned bound can be lowered further in current scenario. Implications of the baryon asymmetry bound on the free parameters ( $T_R, n$ ) of non-standard cosmology is also worth studying.

### 5.1 CP asymmetry

The fermion triplet  $\Sigma_i = \Sigma_{Ri} + \Sigma_{Ri}^c$  is actually composed of three components and in two by two notation it is expressed as

$$\Sigma_i = \begin{pmatrix} \Sigma_i^0/\sqrt{2} & \Sigma_i^+ \\ \Sigma_i^- & -\Sigma_i^0/\sqrt{2} \end{pmatrix}. \quad (5.1)$$

Among these three components ( $\Sigma_i^+, \Sigma_i^0, \Sigma_i^-$ ), the neutral one, which is a Majorana fermion, mimics the behaviour of right handed neutrino as in the case of Type-I seesaw. The charged states,  $\Sigma_i^\pm = \Sigma_{Ri}^\pm + \Sigma_{Ri}^\mp{}^c$ , are the Dirac fermions. Now, due to the  $SU(2)_L$  symmetry, it can be argued that decay widths (to lepton Higgs pair) of all three components should be equal and are given by

$$\Gamma_{\Sigma_i^0} = \Gamma_{\Sigma_i^+} = \Gamma_{\Sigma_i^-} = \frac{M_{\Sigma_i}}{8\pi} |y_\Sigma^\dagger y_\Sigma|_{ii}, \quad (5.2)$$

where ‘ $i$ ’ is the generation index of the triplet. Thus, for our future calculations we will use the notation  $\Gamma_{\Sigma_i}$  (omitting the ‘charge’ index) for the decay width of a specific generation of the triplet irrespective of its charge. It is evident that the thermally averaged decay rate (Eq. (C.2)) becomes three times to that of the well known singlet right handed neutrino, since the equilibrium number density of the decaying triplet (considering the neutral and charged components) is simply three times of the right handed neutrino. The CP asymmetry parameter [88], quantified by the difference between decay rates of ‘heavy triplet to lepton Higgs pair’ and its CP conjugate process, is expressed mathematically as

$$\epsilon_{\Sigma_i} = \frac{\Gamma(\Sigma_i \rightarrow L H) - \Gamma(\bar{\Sigma}_i \rightarrow \bar{L} \bar{H})}{\Gamma(\Sigma_i \rightarrow L H) + \Gamma(\bar{\Sigma}_i \rightarrow \bar{L} \bar{H})}, \quad (5.3)$$

where the asymmetry parameter includes contribution from all three components of the triplet. The generic expression for CP asymmetry produced due to the decay of the next-to-lightest triplet ( $\Sigma_2$ ) is given by [68–70]

$$\epsilon_{\Sigma_2} = \frac{3}{2} \left( \frac{M_{\Sigma_2}}{M_{\Sigma_3}} \right) \left( \frac{\Gamma_{\Sigma_3}}{M_{\Sigma_3}} \right) I_\Sigma \left( \frac{f_v - 2f_s}{3} \right), \quad (5.4)$$

---

<sup>12</sup>This is similar to the Davidson-Ibarra bound [87] obtained in case of singlet, i.e  $M_{N_1} \gtrsim 10^9$  GeV.



where

$$I_\Sigma = \frac{\text{Im} \left[ \left( y_\Sigma^\dagger y_\Sigma \right)_{23}^2 \right]}{|y_\Sigma^\dagger y_\Sigma|_{22} |y_\Sigma^\dagger y_\Sigma|_{33}}$$

and

$$\frac{\Gamma_{\Sigma_3}}{M_{\Sigma_3}} = \frac{|y_\Sigma^\dagger y_\Sigma|_{33}}{8\pi} . \quad (5.5)$$

$f_v$  and  $f_s$  are vertex and self energy correction functions given by

$$f_v = \frac{M_{\Sigma_3}^2 (M_{\Sigma_3}^2 - M_{\Sigma_2}^2)}{(M_{\Sigma_3}^2 - M_{\Sigma_2}^2)^2 + M_{\Sigma_2}^2 \Gamma_{\Sigma_3}^2} , \quad (5.6)$$

$$f_s = 2 \frac{M_{\Sigma_3}^2}{M_{\Sigma_2}^2} \left[ \left( 1 + \frac{M_{\Sigma_3}^2}{M_{\Sigma_2}^2} \right) \ln \left( 1 + \frac{M_{\Sigma_3}^2}{M_{\Sigma_2}^2} \right) - 1 \right] . \quad (5.7)$$

When the triplet mass spectrum is strongly hierarchical, effectively the asymmetry is produced (and survives till present epoch) solely due to the decay of lightest generation of  $\mathbb{Z}_2$  even triplet, which is  $\Sigma_2$  in this case. So we have to deal with  $\epsilon_{\Sigma_2}$  only. For the sake of notational simplicity, from now on we will omit the subscript ‘2’ in  $\epsilon_{\Sigma_2}$ . In strongly hierarchical limit both the above mentioned loop functions reduce to unity. Therefore the expression for CP asymmetry (Eq. (5.4)) simplifies to

$$\begin{aligned} \epsilon_\Sigma &= \frac{3}{2} \frac{M_{\Sigma_2}}{M_{\Sigma_3}} \frac{\Gamma_{\Sigma_3}}{M_{\Sigma_3}} I_\Sigma \left( -\frac{1}{3} \right) \\ &= -\frac{1}{16\pi} \frac{M_{\Sigma_2}}{M_{\Sigma_3}} \frac{\text{Im} \left[ \left( y_\Sigma^\dagger y_\Sigma \right)_{23}^2 \right]}{|y_\Sigma^\dagger y_\Sigma|_{22}} , \end{aligned} \quad (5.8)$$

which is exactly 1/3 of the CP asymmetry obtained from the decay of hierarchical RH neutrinos in case of Type-I seesaw mechanism. Following the same arguments as that of the fermion singlet, the theoretically allowed maximum value of CP asymmetry turns out to be [68–70]

$$\begin{aligned} \epsilon_\Sigma^{\text{max}} &= \frac{M_{\Sigma_2}}{8\pi v^2} (m_3 - m_1) \\ &= \frac{M_{\Sigma_2}}{8\pi v^2} \left( \frac{\Delta m_{31}^2}{m_3 + m_1} \right) , \end{aligned} \quad (5.9)$$

where  $m_i (i = 1, 2, 3)$  are the light neutrino mass eigenvalues<sup>13</sup> and  $v (= 246\text{GeV})$  is the SM VEV. To get an estimate for the lowest value of  $M_{\Sigma_2}$  that can produce adequate asymmetry to meet the observed value of baryon asymmetry, this above mentioned upper limit of CP asymmetry has to be used in the Boltzmann equations. A few earlier studies [68–70] dealing with fermion triplet leptogenesis have shown that the concerned lower limit on the mass of the lightest triplet lies near  $10^{11}$  GeV.

<sup>13</sup>Since two triplet fermions take part in the active neutrino mass generation so the mass of the lightest component among the active neutrinos would be zero, i.e.,  $m_1 = 0$ .

## 5.2 Boltzmann equations for leptogenesis in standard cosmology

The set of Boltzmann equations are used to track the evolution of lepton asymmetry with temperature as the Universe gradually cools down. Let us define few important parameters, necessary for writing the Boltzmann equations. Instantaneous abundance of a particle species is conventionally expressed in terms of scaled number density  $Y_a(z)(= \frac{n_a(z)}{s(z)})$ , where  $n_a(z)$  is the number density of the particle species ‘ $a$ ’,  $s(z)$  is the entropy density and  $z$  is a dimensionless parameter ( $z = M_{\Sigma_2}/T$ )<sup>14</sup> varying inversely with the temperature of the Universe. Since all three components of the triplet contribute equally to the asymmetry, it would be more convenient to handle the set of Boltzmann equations in terms of total number density of a specific triplet generation, i.e  $n_{\Sigma_i} = n_{\Sigma_i^0} + n_{\Sigma_i^+} + n_{\Sigma_i^-}$ . In the present case, the asymmetry is assumed to be generated solely due to the decay of  $\Sigma_2$ . Therefore we are concerned with the number density  $n_{\Sigma_2}$  only<sup>15</sup>. Since there is no other generation of the triplet involved in the Boltzmann equations, we can safely use the notation  $n_{\Sigma}$  for  $n_{\Sigma_2}$ . The evolution of the triplet abundance and the corresponding  $(B - L)$  asymmetry are governed by the following set of Boltzmann equations [70]

$$sH z \frac{dY_{\Sigma}}{dz} = -\gamma_D \left( \frac{Y_{\Sigma}}{Y_{\Sigma}^{eq}} - 1 \right) - 2\gamma_A \left( \frac{Y_{\Sigma}^2}{Y_{\Sigma}^{eq2}} - 1 \right), \quad (5.10)$$

$$sH z \frac{dY_{B-L}}{dz} = -\gamma_D \epsilon_{\Sigma} \left( \frac{Y_{\Sigma}}{Y_{\Sigma}^{eq}} - 1 \right) - \frac{Y_{B-L}}{Y_l^{eq}} \left( \frac{\gamma_D}{2} + \gamma_{\Sigma}^{sub} \right), \quad (5.11)$$

where  $\gamma$  generically designates the reaction density<sup>16</sup> of the process under consideration and the subscript ‘ $D$ ’ denotes the decay process, whereas ‘ $A$ ’ stands for  $2 \rightarrow 2$  gauge boson mediated scattering processes. The  $\gamma_{\Sigma}^{sub}$  term accounts for the contribution from  $\Delta L = 2$  scattering processes where the resonant contribution has already been subtracted. It is clear from the above set of Boltzmann equations that there is an extra term (compared to that of Type-I seesaw) involving  $\gamma_A$  in the first equation. It appears since the fermion triplet can couple to the gauge bosons unlike the gauge singlet fermions. The above set of Boltzmann equations can be rewritten in a convenient form as

$$\frac{dY_{\Sigma}}{dz} = -D(z) (Y_{\Sigma}(z) - Y_{\Sigma}^{eq}(z)) - S_A(z) (Y_{\Sigma}(z)^2 - Y_{\Sigma}^{eq}(z)^2), \quad (5.12)$$

$$\frac{dY_{B-L}}{dz} = -\epsilon_{\Sigma} D(z) (Y_{\Sigma}(z) - Y_{\Sigma}^{eq}(z)) - (W(z) + W^{sub}(z)) Y_{B-L}(z), \quad (5.13)$$

where different decay and scattering terms are restructured and can be expressed in terms of some fundamental constants and parameters of the model as follows. Decay ( $D$ ) term and

<sup>14</sup>We have used this definition of  $z$  only for leptogenesis analysis. It should not be confused with the  $z$  used in analysis of DM.

<sup>15</sup>Expressions for equilibrium number densities of different particle species are given in Appendix B.

<sup>16</sup>Detailed expression is given in Appendix C.

gauge boson mediated scattering ( $S_A$ ) terms are simplified as

$$\begin{aligned}
D(z) &= \frac{\gamma_D(z)}{s(z)H(z)zY_\Sigma^{eq}(z)} \\
&= \frac{n_\Sigma^{eq}(z)\Gamma_\Sigma \frac{K_1(z)}{K_2(z)}}{s(z)H(z)z \frac{n_\Sigma^{eq}(z)}{s(z)}} \\
&= \left( \frac{M_{pl}}{8\pi v^2 1.66 g_*^{1/2}} \right) \tilde{m} z \frac{K_1(z)}{K_2(z)}
\end{aligned} \tag{5.14}$$

where  $\tilde{m} = 8\pi\Gamma_\Sigma \frac{v^2}{M_{\Sigma_2}^2}$ . The thermal reaction rate of gauge boson mediated two body scattering process  $\gamma_A$ , involves integral of the reduced cross-section ( $\hat{\sigma}$ ), of the relevant process, over the centre of mass energy of the initial particles, is computed as

$$\begin{aligned}
\gamma_A(z) &= \frac{M_{\Sigma_2}^4}{64\pi^4 z} \int_{x_{min}}^{\infty} \sqrt{x} K_1(z\sqrt{x}) \hat{\sigma}_A(x) dx \\
&= \frac{M_{\Sigma_2}^4}{64\pi^4 z} I(z),
\end{aligned} \tag{5.15}$$

where,

$$I(z) = \int_{x_{min}}^{\infty} \sqrt{x} K_1(z\sqrt{x}) \hat{\sigma}_A(x) dx,$$

and the integration variable  $x$  is defined as the ratio of centre of mass energy ( $s$ ) to the square of decaying particle's mass ( $M_{\Sigma_2}$ ). The minimum value of centre of mass energy for a generic two body process ( $a, b \rightarrow i, j, \dots$ ) is given by  $s_{min} = \max [(m_a + m_b)^2, (m_i + m_j + \dots)^2]$ . The analytical expression for the reduced cross-section is given in Appendix D. The gauge mediated scattering term ( $S_A$ ) of Eq. (5.12) can be written as a function of the above mentioned integral as

$$\begin{aligned}
S_A(z) &= \frac{2\gamma_A(z)}{s(z)H(z)zY_\Sigma^{eq}(z)^2} \\
&= \left( \frac{\pi^2 g_*^{1/2} M_{pl}}{1.66 \times 180 g_\Sigma^2} \right) \frac{1}{M_{\Sigma_2}} \left( \frac{I(z)}{z K_2(z)^2} \right),
\end{aligned} \tag{5.16}$$

where  $g_\Sigma$  is the internal degrees of freedom of the Majorana type fermion triplet  $\Sigma$ . Similarly the washout terms ( $W$  and  $W^{sub}$  of Eq. (5.13)) due to inverse decay and  $\Delta L = 2$  scattering (off-shell) processes are given by

$$W(z) = \left( \frac{3M_{pl}}{1.66 \times 32\pi v^2 g_*^{1/2}} \right) \tilde{m} z^3 K_1(z), \tag{5.17}$$

$$\begin{aligned}
W^{sub}(z) &= \left( \frac{M_{pl}}{1.66 \times 64\pi^2 g_*^{1/2}} \right) \frac{z^3}{M_{\Sigma_2}} \left\{ \int_{x_{min}}^{\infty} \sqrt{x} K_1(z\sqrt{x}) (\hat{\sigma}_s(x) + \hat{\sigma}_t(x)) dx \right\} \\
&= \left( \frac{M_{pl}}{1.66 \times 64\pi^2 g_*^{1/2}} \right) \frac{z^3}{M_{\Sigma_2}} (I_s(z) + I_t(z))
\end{aligned} \tag{5.18}$$

with  $I_s, I_t$  being integral of the  $s$  channel<sup>17</sup> and  $t$  channel (reduced) cross-sections.

### 5.2.1 Baryon asymmetry and efficiency factor at present epoch

At relatively lower (than the leptogenesis scale, i.e  $T \ll M_{\Sigma_2}$ ) temperature (or equivalently  $z \gg 1$ ) when the strength of lepton/baryon number violating interactions become negligibly small,  $Y_{B-L}$  freezes to a certain value and remains constant till the present epoch. Assuming vanishing preexisting asymmetry (i.e  $Y_{B-L}(z_i) = 0$ ) the set of Boltzmann equations (Eqs. (5.12 and 5.13)) can be solved up to a arbitrary value of  $z$  to obtain

$$Y_{B-L}(z) = -\epsilon_{\Sigma} Y_{\Sigma}^{eq}(z \ll 1) \left\{ -\frac{1}{Y_{\Sigma}^{eq}(z \ll 1)} \int_{z_i}^z dz' \frac{dY_{\Sigma}}{dz'} e^{-\int_{z'}^z (W(z'') + W^{sub}(z'')) dz''} \right\} \\ = -\epsilon_{\Sigma} Y_{\Sigma}^{eq}(z \ll 1) \kappa(z), \quad (5.19)$$

where the integral inside the curly bracket gives efficiency factor evaluated at any arbitrary  $z$ . If we assume  $z_f$  to be the value of  $z$  where  $B-L$  asymmetry gets frozen, i.e

$$Y_{B-L}(z_f) = -\epsilon_{\Sigma} Y_{\Sigma}^{eq}(z \ll 1) \kappa(z_f) \\ \text{or, } Y_{B-L}^f = -\epsilon_{\Sigma} Y_{\Sigma}^{eq}(z \ll 1) \kappa^f. \quad (5.20)$$

The so called sphaleron process converts this frozen value of  $B-L$  asymmetry to baryon asymmetry which is connected to  $Y_{B-L}^f$  through the multiplicative sphaleron transition factor  $a_{sph} = 28/79$ , i.e,

$$Y_B(z) = a_{sph} Y_{B-L}(z) = -a_{sph} \epsilon_{\Sigma} Y_{\Sigma}^{eq}(z \ll 1) \kappa(z) \quad \text{and} \quad (5.21)$$

$$Y_B^f = a_{sph} Y_{B-L}(z_f) = -a_{sph} \epsilon_{\Sigma} Y_{\Sigma}^{eq}(z \ll 1) \kappa^f. \quad (5.22)$$

The viability of our model can be tested through a comparison between the theoretically predicted value of baryon asymmetry ( $Y_B^f$ ) with the observed one ( $Y_B^{obs}$ ) which ranges between  $8.9 \times 10^{-11} < Y_B^{obs} < 9.2 \times 10^{-11}$  at 95% confidence level [6].

### 5.2.2 Modification of the Boltzmann equations in non-standard cosmology

It has already been mentioned in Sec. 4.2 that, in non-standard cosmological scenario the Hubble parameter is modified due to the non-trivial contribution of the  $\phi$  field in total energy density. It is well known that above the scale of electroweak (EW) symmetry breaking all the SM particles can be treated to be relativistic and thereby allows us to assume  $g_*(T > T_{EW}) = g_{SM} \simeq 106.75$ . Since the processes relevant to generation and washout of lepton asymmetry take place much above the EW scale,  $g_*(T)$  in that temperature regime behaves as a constant with a value  $g_{SM}$ . In present scenario the total energy density (Eq. (4.9)) includes additional (apart from the well known radiation energy) temperature dependent terms involving non-standard parameters  $T_r, n$ . It affects the Hubble parameter directly by introducing a steeper temperature dependence as already shown in Eq. (4.12), i.e  $H(z) = H_{rad}(z) f(z, z_r, n)$  (with  $f(z, z_r, n) > 1$ ). The particle physics inputs (i.e decay widths and scattering cross-sections) in the Boltzmann equations are totally unaffected by the changes incorporated in the cosmology. Therefore it can be stated unambiguously that in spite of introduction of modified cosmology,

<sup>17</sup>The resonance contribution has been properly subtracted for the  $s$  channel process. Analytical expressions for  $\hat{\sigma}_s(x), \hat{\sigma}_t(x)$  are given in Appendix D.

the basic structure of the Boltzmann equations (Eqs. (5.12 and 5.13)) remains unaltered, except the decay and scattering terms which are modulated by non-standard effects through a  $z$  dependent term. Lets us first inspect the non-trivial modification in the decay term, i.e.

$$\begin{aligned}\tilde{D}(z) &= \frac{\gamma_D(z)}{s(z)H(z)zY_{\Sigma}^{eq}(z)} \\ &= \left( \frac{\gamma_D(z)}{s(z)H_{rad}(z)zY_{\Sigma}^{eq}(z)} \right) \frac{1}{f(z, z_r, n)}, \\ &= \frac{D(z)}{f(z, z_r, n)}.\end{aligned}\tag{5.23}$$

Analogy between the structure of various decay and scattering terms guide us to realize that all the concerned terms ( $D, S_A, W, W^{sub}$ ) will be modified (to  $\tilde{D}, \tilde{S}_A, \tilde{W}, \tilde{W}^{sub}$ ) exactly in a similar manner through the common multiplicative factor  $1/f(z, z_r, n)$ , where

$$f(z, z_r, n) = \left[ 1 + \left( \frac{g_*(M_{\Sigma_2}/z)}{g_*(M_{\Sigma_2}/z_r)} \right)^{\frac{1+n}{3}} \left( \frac{z_r}{z} \right)^n \right]^{1/2}.\tag{5.24}$$

Thus, in order to find the baryon (precisely  $B - L$ ) asymmetry produced due to the decay of a heavy fermionic triplet in a non-standard cosmological scenario, we have to solve the same set of Boltzmann equations (Eqs. (5.12 and 5.13)) with modified decay and scattering terms ( $\tilde{D}, \tilde{S}_A, \tilde{W}, \tilde{W}^{sub}$ ).

### 5.3 Analysis of numerical results: constraining the non-standard parameters

The present study of fermion triplet leptogenesis in non-standard cosmology is mainly motivated to inspect the following intriguing issues: (i) possibility of producing observed asymmetry at some lower mass scale, (ii) whether baryon asymmetry bound can impose a more stringent constraint on the non-standard parameters which are already restricted by the DM relic density bound. It is worth mentioning that, since we are interested to find the lower limit (using BAU) on  $M_{\Sigma_2}$ , we should use theoretically possible maximum value of the CP asymmetry parameter. So we have used  $\epsilon_{\Sigma}^{\max}$  (Eq. (5.9)) as the CP asymmetry throughout the analysis (for both standard and non-standard case).

Let us proceed with a brief discussion on the scheme of solution of Boltzmann equations (Eq. (5.12), Eq. (5.13)) in non-standard cosmology (i.e, using  $\tilde{D}, \tilde{S}_A, \tilde{W}, \tilde{W}^{sub}$ ). Although in standard cosmology scenario the decay/inverse decay and the scattering terms, have been expressed as explicit functions of  $z$ , they depend on other parameters like  $\tilde{m}$  and  $M_{\Sigma_2}$  too. However in modified cosmological scenario (along with the standard ones) the non-standard parameters play a pivotal role in determining the decay/inverse decay and scattering terms. Therefore they ( $\tilde{D}, \tilde{S}_A, \tilde{W}, \tilde{W}^{sub}$ ) become functions of  $(z; \tilde{m}, M_{\Sigma_2}, T_r, n)$  where  $z$  is the integration variable and others are parameters of the model. It is worthwhile to mention that we have kept  $\tilde{m}$  fixed at a benchmark value 0.05 eV throughout the analysis, whereas the other parameters are varied within suitable range to answer the questions raised in the first paragraph of this section.

At first we solve the Boltzmann equations for leptogenesis assuming standard radiation dominated cosmology for fixed value of triplet mass  $M_{\Sigma_2}$ . We show the variation of  $Y_B$

with  $z$  (in left panel of Fig. (8)) to get an estimate of the specific value of  $z$  above which the asymmetry freezes. The same exercise is repeated taking into account the presence of non-standard terms in the Boltzmann equations. The evolution of  $Y_B$  is shown in the same plot together with its standard counter part. The figure (left panel, Fig. (8)) vividly shows

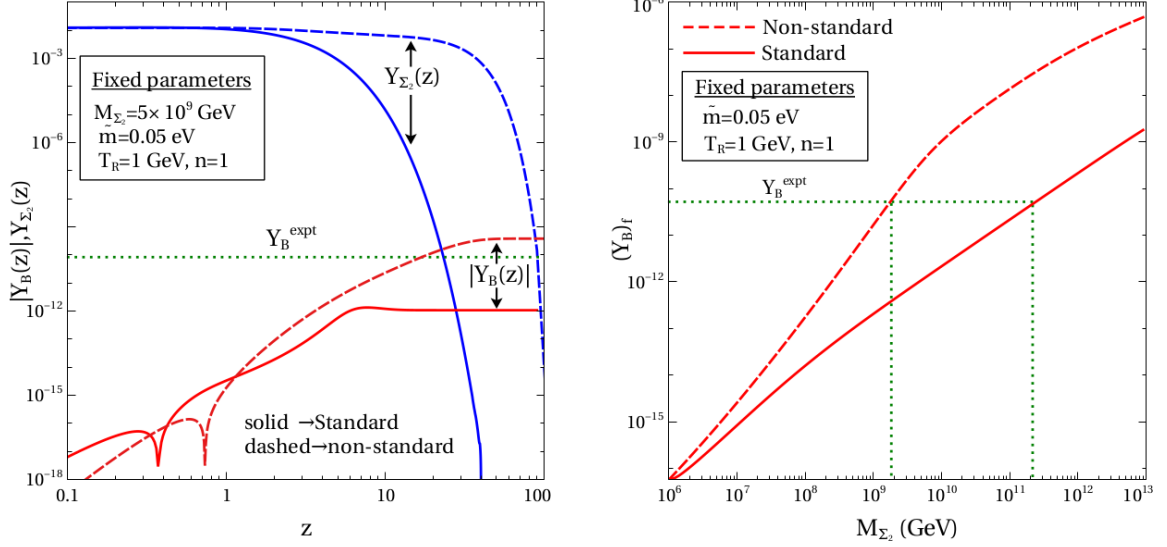


**Figure 8. Left:** Evolution of baryon asymmetry  $Y_B$  (red line) and triplet abundance  $Y_{\Sigma_2}$  (blue line) with  $z$  assuming standard (solid line) as well as non-standard (dashed line) cosmology for fixed benchmark value of set of parameters as ( $M_{\Sigma_2} = 5 \times 10^9 \text{ GeV}$ ,  $\tilde{m} = 0.05 \text{ eV}$ ,  $T_r = 1 \text{ GeV}$ ,  $n = 1$ ). Horizontal dotted line represents the experimental value of baryon asymmetry. **Right:** Variation of final (or frozen) value of baryon asymmetry ( $Y_B^f$ ) with mass of the decaying triplet ( $M_{\Sigma_2}$ ) for fixed values of the set of parameters ( $\tilde{m} = 0.05 \text{ eV}$ ,  $T_r = 1 \text{ GeV}$ ,  $n = 1$ ). The particular points, where the vertical dotted lines have touched the abscissa, denote the lowest value of  $M_{\Sigma_2}$  for which the BAU bound can be satisfied.

that, for chosen set of parameters the final asymmetry indeed freezes to a higher value in non-standard case. To investigate about the nature of dependence of final asymmetry ( $Y_B^f$ ) on the decaying triplet mass ( $M_{\Sigma_2}$ ), we solve the Boltzmann equations for a continuous range of  $M_{\Sigma_2}$ . The final asymmetry (for standard as well as non-standard) is plotted (right panel Fig. (8)) against  $M_{\Sigma_2}$ , while the other parameters ( $\tilde{m}, T_r, n$ ) are kept fixed at a benchmark value ( $\tilde{m} = 0.05 \text{ eV}$ ,  $T_r = 1 \text{ GeV}$ ,  $n = 1$ ). As anticipated,  $Y_B^f$  for both the plots shows monotonically increasing behaviour. However, the non-standard curve (denoted by dashed line) shows a steeper dependence, thereby satisfying the baryon asymmetry bound at a much lower (approximately 2 orders) value of  $M_{\Sigma_2}$  compared to the standard one. So we have got the answer of our first question, i.e the lower bound on  $M_{\Sigma_2}$  indeed decreases in presence of non-standard effect.

Let us recall the relation between final value of baryon asymmetry and efficiency factor, i.e

$$Y_B^f(M_{\Sigma_2}, \tilde{m}, T_r, n) = -a_{\text{sph}} \epsilon_{\Sigma}(M_{\Sigma_2}) Y_{\Sigma}^{\text{eq}}(z \simeq 0) \kappa^f(M_{\Sigma_2}, \tilde{m}, T_r, n) \quad (5.25)$$

where we have shown explicit dependence on model parameters. In principle this functional dependence indicates that final asymmetry expected to vary with the non-standard param-

ters  $(T_r, n)$  even if  $M_{\Sigma_2}$  is kept fixed. Therefore the conclusion drawn towards the end of last paragraph may not be true for all combinations of  $(T_r, n)$ . To examine its validity for other (than those used to draw the Fig. (8)) values of ‘ $n$ ’ we redraw the same plot (i.e  $Y_B^f$  vs  $M_{\Sigma_2}$ ) for three sample values of  $n$  and show them in the left panel of Fig. (9). It is observed that

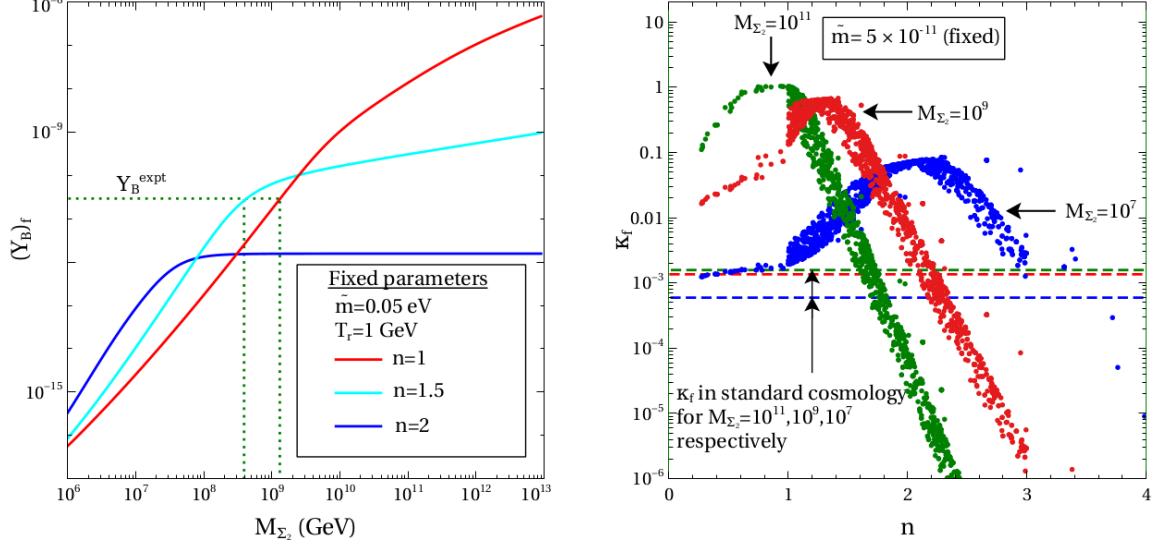


**Figure 9. Left:** Variation of final (or frozen) value of baryon asymmetry ( $Y_B^f$ ) with mass of the decaying triplet ( $M_{\Sigma_2}$ ) for three benchmark values of non-standard parameters  $n$  while  $\tilde{m}$  and  $T_r$  kept fixed throughout. The lower limit on  $M_{\Sigma_2}$  decreases up to  $n = 1.5$ . **Right:** Dependence of efficiency factor ( $\kappa^f$ ) on the non-standard parameter  $n$  for three sample values of  $M_{\Sigma_2}$ . Horizontal dashed lines represent the corresponding efficiency factor in standard cosmology (obviously it does not depend on  $n$ ).  $M_{\Sigma_2}$  and  $\tilde{m}$  are in GeV unit.

the said lower limit on  $M_{\Sigma_2}$  decreases with  $n$  only up to a certain value of  $n$  (which is  $n = 1.5$  in this case), further increment in  $n$  results in a drastic fall of final asymmetry which implies increment of the lower bound of  $M_{\Sigma_2}$ . This observation allows us to state unambiguously that the said lower bound can not be lowered indefinitely by increasing  $n$ . There exists a critical value of  $n$  (for each fixed value of  $M_{\Sigma_2}$ ) beyond which the final asymmetry declines monotonically. A deeper understanding about the nature of efficiency factor is required to shed some light on this issue. Eq. (5.25) clearly designates that the non-standard parameters only affect the efficiency factor, whereas the CP asymmetry parameter being solely dictated by the underlying particle physics model remains unaffected. Variation of efficiency factor ( $\kappa^f$ ) with  $n$  for three different fixed values of  $M_{\Sigma_2}$  is depicted in the right panel of Fig. (9). The efficiency factors obtained using standard cosmology (for same three benchmark values of  $M_{\Sigma_2}$ ) have been shown in the same figure with horizontal dashed lines. It is to be noted that the efficiency factor is indeed enhanced in non-standard case, but above a certain value of ‘ $n$ ’ it again starts to decrease and may become even lesser than its standard counterpart. This peculiar behaviour of  $\kappa^f$  can be explained by studying the effect of non-standard parameters (specially  $n$ ) on the terms responsible for the creation and washout of asymmetry. The integral representation (Eq. (5.19)) of efficiency factor  $\kappa$  clearly indicates its dependence on ‘rate<sup>18</sup> of change of  $Y_\Sigma$ ’ and ‘the integral over washout terms’. It can be understood from

<sup>18</sup>This rate is again proportional to Decay and scattering terms (Eq. (5.12))



Eq. (5.23), that the decay term  $\tilde{D}$  (and also  $\tilde{S}_A, \tilde{W}, \tilde{W}^{sub}$ ) decreases with increase in  $n$ . When  $n$  is increased from zero, initially the effect of decrease in washout (effectively increase in the integral) surpluses decrease in the Decay and scattering terms. Thus the resultant effect becomes positive which implies increment in the efficiency factor. However, beyond a critical value of  $n$  the decrement in the  $\tilde{D}$  and  $\tilde{S}_A$  dominates overwhelmingly driving the efficiency factor towards a lower value.

The remarkable feature of this study is the interrelation, between DM phenomenology and leptogenesis, which is brought about by the non-standard parameters. These parameters have taken a crucial role in producing the correct relic abundance within the experimentally allowed range of  $M_{\Sigma_1}$  as well as playing a vital role in bringing down the lower limit on  $M_{\Sigma_2}$  (required for successful prediction of BAU). In this context, it should be mentioned that during the computation of DM relic density, the non-standard parameters are varied within the range  $10^{-3} \leq T_r(\text{GeV}) \leq 10$  and  $0 \leq n \leq 5$  while the mass of DM ( $M_{\Sigma_1}$ ) is taken between 500 and 1500 GeV. Moreover, we have also imposed the bound on DM relic density in  $3\sigma$  range as obtained by the Planck collaboration i.e.,  $0.1172 \leq \Omega_{DM} h^2 \leq 0.1226$ . For leptogenesis, we have solved the Boltzmann equations for the entire range of  $(T_r - n)$  values previously allowed by relic density bound, while  $M_{\Sigma_2}$  has been varied independently over a wide range ( $10^6 - 10^{13}$ ) GeV. It can be inferred from the relevant plot (left panel, Fig. (10)) that the parameter space (in  $(T_r - n)$  plane) allowed by the relic density bound, shown by deep green points, has shrunk significantly to a smaller region consisting of deep red points upon imposition of second round of constraint, i.e. the BAU bound. For the sake of completeness we scan the whole allowed parameter space (by BBN bound + DM relic bound + Baryon asymmetry bound) and compute the maximum possible value of total energy density ( $\rho_{\text{tot}}$ ) (using Eq. (4.9)) in our model. The typical combinations of  $(T_r, n, M_{\Sigma_2})$  which result in  $\rho_{\text{tot}} > \rho_{\text{max}}$ <sup>19</sup>, where  $\rho_{\text{max}}$  is the maximum allowed energy density of the Universe after inflation as dictated by the Planck data [6], are indicated by the magenta patch. Further in-depth studies related to leptogenesis, like mass ( $M_{\Sigma_2}$ ) distribution in  $(T_r - n)$  plane, have to be done using this common parameter space designated by the deep red patch in the above mentioned plot.

The meticulous analysis of numerical results, done so far conveys a clear message that dependence of final baryon asymmetry  $Y_B^f$  on  $M_{\Sigma_2}$  and other non-standard parameters is quite convoluted. Even the nature of dependence on a particular parameter (while others are kept fixed) is not always monotonic. Nevertheless, to get a comprehensive picture of the three dimensional parameter space (spanned by  $M_{\Sigma_2}, T_r, n$ ) allowed by recent experimental bound on BAU (as well as relic density bound), we depict<sup>20</sup>  $\log_{10}(M_{\Sigma_2})$  with continuously varying colours in  $\log_{10}(T_r) - n$  plane (right panel, Fig. (10)). The vertical colour bar contains all the required numerical information about the representative colours. The right most allowed region (deep cyan) corresponding to  $M_{\Sigma_2} \sim 10^{12}$  GeV has been covered by the magenta patch which indicates that strict adherence with the Planck bound on total energy density will lead to exclusion of this narrow region from the allowed parameter space. However, the region associated with the lower values of  $M_{\Sigma_2}$  remains absolutely unaffected (by the  $\rho_{\text{max}}$  bound). The deep brown patch in the figure signifies that the lowest value of

<sup>19</sup>The maximum allowed energy density[89] of the Universe (as suggested by Planck data [6]) after the inflation era is given by  $\rho_{\text{max}} \sim 10^{66} \text{ GeV}^4$ .

<sup>20</sup>Only those combinations of  $M_{\Sigma_2}, T_r, n$  are considered which produces  $Y_B^f$  within the experimental range.

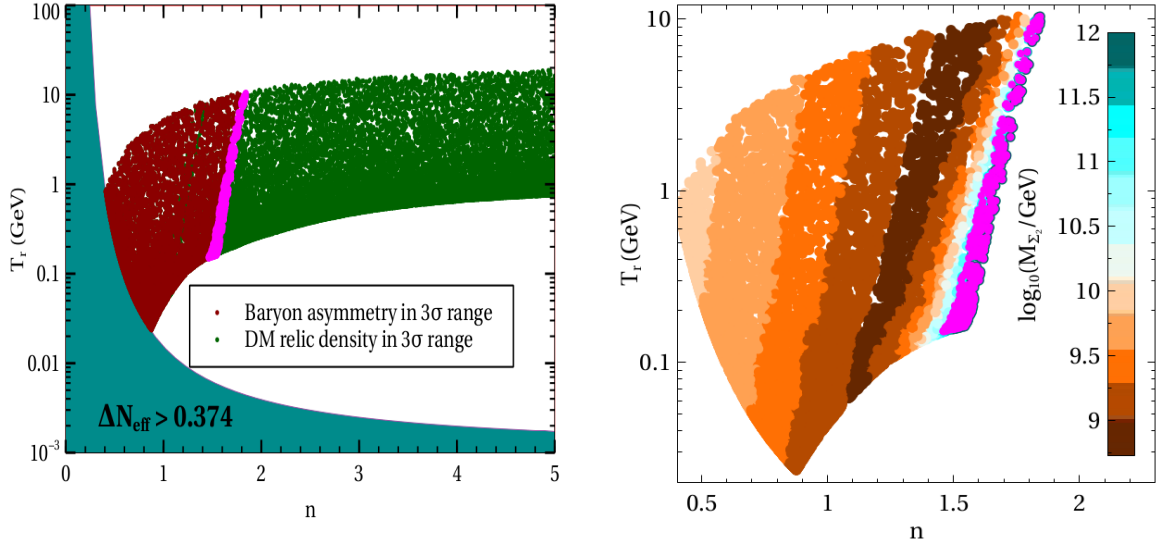


**Figure 10.** **Left:** Non-standard parameter space ( $T_r - n$ ) allowed by relic density bound is denoted by deep green points whereas deep red points are those which satisfy both relic density as well as baryon asymmetry bound. The narrow magenta patch (which has actually covered few points in the dark red region) denotes those typical combinations of  $(T_r, n, M_{\Sigma_2})$  which produce total energy density greater than the Planck limit. The area painted in deep cyan stands for the region excluded by BBN bound. The plot shows that the imposition of BAU bound reduces the allowed parameter space considerably. **Right:** Allowed (by BAU bound) values of  $M_{\Sigma_2}$  are represented by different colours in  $(T_r - n)$  plane. The vertical colour bar stands for specific numerical values of  $M_{\Sigma_2}$  as denoted by different colours. It can be seen that the magenta patch has overshadowed the allowed high mass region to some extent. This narrow region, although allowed by the baryon asymmetry bound, is in tension with the Planck constraint on the total energy density ( $\rho_{\max} \sim 10^{66} \text{ GeV}^4$ ). However, the low mass region is completely safe from this bound. The deep brown patch signifies the lowest achievable value of  $M_{\Sigma_2}$ , using non-standard cosmology which is  $\lesssim 10^9 \text{ GeV}$ .

the decaying triplet mass, for which BAU bound can be satisfied, is less than  $10^9 \text{ GeV}$ , while  $1.0 \lesssim n \lesssim 1.6$  and  $T_r$  is less restricted, can take any value between  $(1 - 10) \text{ GeV}$ . Further increment/decrement in  $n$  will shift lower bound on  $M_{\Sigma_2}$  towards higher value.

## 6 Summary and Conclusion

In this work, we have considered the Type-III seesaw model where the SM is extended by three  $\text{SU}(2)_L$  fermion triplets to generate tiny Majorana masses for the SM neutrinos. However, here we have imposed a  $\mathbb{Z}_2$  symmetry on one of the triplet fermions  $\Sigma_{R1}$  and accordingly, the neutral component of  $\Sigma_{R1}$  becomes a stable dark matter candidate and one active neutrino remains massless. On the other hand, the heavier generations of the newly introduced triplet fermions can couple to the SM Higgs and leptons through Yukawa coupling, which in turn opens up the possibility to account for the observed baryon asymmetry of the Universe through CP violating out of equilibrium decay of triplet fermions to lepton Higgs pair.

It is worthwhile to mention that although the stability of the proposed DM candidate ( $\Sigma_1^0$ ) has been ensured by the imposed  $\mathbb{Z}_2$  symmetry, it remains under-abundant throughout the entire mass range (of  $M_{\Sigma_1}$ ) allowed by the indirect and collider searches of DM. Assuming the evolution of the relic abundance through standard radiation dominated cosmology, it can be shown that the correct relic density can be obtained for a fermion triplet DM of mass  $\sim 2.3$  TeV which is ruled out unambiguously by the indirect searches of DM. To alleviate this problem or in other words to achieve the correct relic abundance for a relatively lower mass (allowed by experimental results) of the triplet, we resort to a typical form of non-standard cosmology where primordial (well above the BBN temperature) Universe expands faster than the standard picture. In the present work we have shown that, indeed it is possible to produce the correct relic abundance for a triplet mass as low as a few hundreds of GeV while the values of the non-standard parameters ( $T_r - n$ ) have been chosen judiciously.

From the point of view of particle physics, it seems that the dark sector and the Yukawa sector (responsible for asymmetry generation) are disconnected by the  $\mathbb{Z}_2$  symmetry whereas the modified cosmology is bridging this gap through its parameters  $T_r - n$ . These two parameters play a key role in getting correct relic abundance of the DM as well as producing BAU in agreement with recent data. It has been found in our analysis that although the DM relic abundance constraint can be satisfied for high values of  $n$  (up to the maximum value used for scanning the parameter space), the baryon asymmetry bound restricts it to be  $\lesssim 1.8$ . On the other hand, the relic density constraint bounds  $n$  from below with a limiting value of 0.4. Thus it can be concluded that simultaneous satisfaction of DM relic density bound and BAU bound imposes a stringent restriction on the common parameter space spanned by the non-standard parameters  $T_r - n$ . The exhaustive analysis of leptogenesis leads us to another noteworthy result, i.e, the lower bound on triplet mass (obtained from the observed BAU) can be brought down further by two orders of magnitude in comparison to the bound estimated using standard cosmology.

## Acknowledgements

The research of AB is supported by the National Research Foundation of Korea (NRF) funded by the Ministry of Education through the Center for Quantum Space Time (CQUeST) with grant number 2020R1A6A1A03047877 and by the Ministry of Science and ICT with grant number 2021R1F1A1057119. He also acknowledges the support from National Research Foundation grants funded by the Korean government (NRF-2021R1A4A2001897). M.C would like to acknowledge the financial support provided by SERB-DST, Govt. of India through the NPDF project PDF/2019/000622. This work used the Scientific Compute Cluster at GWDG, the joint data center of Max Planck Society for the Advancement of Science (MPG) and University of Göttingen. The authors would like to acknowledge the useful discussion with Laura Covi.

## A Thermal averaged cross-section

In this Appendix, we have listed the expressions of all annihilation and co-annihilation cross sections in the  $s$ -wave approximation as given in Ref. [34],

$$\sigma v_{\Sigma_1^0 \Sigma_1^0} \simeq \frac{2\pi\alpha_L^2}{M_{\Sigma_1}^2}, \quad \sigma v_{\Sigma_1^0 \Sigma_1^\pm} \simeq \frac{29\pi\alpha_L^2}{8M_{\Sigma_1}^2}, \quad \sigma v_{\Sigma_1^+ \Sigma_1^-} \simeq \frac{37\pi\alpha_L^2}{8M_{\Sigma_1}^2}, \quad \sigma v_{\Sigma_1^\pm \Sigma_1^\pm} \simeq \frac{\pi\alpha_L^2}{M_{\Sigma_1}^2}. \quad (\text{A.1})$$

The effective thermal averaged cross-section can be found easily using Eq. (4.2) as

$$\begin{aligned} \langle \sigma v \rangle_{\text{eff}} &= \frac{g_{\Sigma_1^0}^2}{g_{\text{eff}}^2} \sigma v_{\Sigma_1^0 \Sigma_1^0} + 2 \frac{g_{\Sigma_1^\pm}^2}{g_{\text{eff}}^2} \left[ \sigma v_{\Sigma_1^\pm \Sigma_1^\pm} + \sigma v_{\Sigma_1^+ \Sigma_1^-} \right] (1 + \epsilon)^3 \exp(-2\epsilon x) \\ &\quad + 4 \frac{g_{\Sigma_1^0} g_{\Sigma_1^\pm}}{g_{\text{eff}}^2} \sigma v_{\Sigma_1^0 \Sigma_1^\pm} (1 + \epsilon)^{3/2} \exp(-\epsilon x), \end{aligned} \quad (\text{A.2})$$

where  $g_{\Sigma_1^0} = g_{\Sigma_1^\pm} = 2$ ,  $\epsilon = \frac{\Delta}{M_{\Sigma_1}}$ ,  $g_{\text{eff}} = g_{\Sigma_1^0} + 2 g_{\Sigma_1^\pm} (1 + \epsilon)^{3/2} \exp(-\epsilon x)$  and  $\Delta = M_{\Sigma_1^\pm} - M_{\Sigma_1} \simeq 166$  MeV for  $M_{\Sigma_1} \sim 1$  TeV. So  $\epsilon$  turns out to be negligibly small ( $\sim 10^{-4}$ ). Thus in the limit  $\epsilon \rightarrow 0$ , the effective annihilation cross-section (Eq. (A.2)) can be approximated to be

$$\langle \sigma v \rangle_{\text{eff}} \simeq \frac{111}{36} \frac{\pi\alpha_L^2}{M_{\Sigma_1}^2}. \quad (\text{A.3})$$

## B Equilibrium number density and freeze-out temperature

**Number density of different species:** The number density of fermion triplet (for each generation) in terms of temperature (or equivalently  $z = M_\Sigma/T$ ) is given by

$$n_\Sigma^{\text{eq}}(T) = \frac{3}{4} \zeta(3) \frac{g_\Sigma T^3}{2\pi^2} \left( \frac{M_\Sigma}{T} \right)^2 K_2 \left( \frac{M_\Sigma}{T} \right), \quad (\text{B.1})$$

where  $\zeta$  is the Riemann zeta function and  $g_\Sigma$  is the internal degrees of freedom for the triplet fermion. In this case  $g_\Sigma = 2 + 4 = 6$ , where the factor 2 is for the Majorana fermion (neutral component) and the factor 4 is for the Dirac fermion (charged component) respectively. Similarly number density of SM doublet leptons is

$$n_l^{\text{eq}}(T) = \frac{3}{4} \zeta(3) \frac{g_l T^3}{\pi^2}, \quad (\text{B.2})$$

and that of photons is

$$n_\gamma^{\text{eq}}(T) = \zeta(3) \frac{g_\gamma T^3}{\pi^2}, \quad (\text{B.3})$$

where  $g_\gamma = g_l = 2$  (since leptons can be treated to be massless above EW symmetry breaking scale).

Co-moving entropy density as a function of temperature is expressed as

$$s(T) = \frac{2\pi^2}{45} g_* T^3, \quad (\text{B.4})$$

where  $g_*$  is number of effective relativistic degrees of freedom which turns out to be  $\simeq 106.75$  if all Standard Model particles are assumed to be relativistic.

**Freeze-out temperature in non-standard cosmology:** The dark matter gets thermally decoupled from the plasma at a specific temperature  $T_f$  (or equivalently  $z_f (= M_{\Sigma_1}/T_f)$ ) whenever the equality

$$H(z_f) = n_{\Sigma_1^0}^{eq}(z_f) \langle \sigma v \rangle_{\text{eff}} \quad (\text{B.5})$$

is reached. Using the modified Hubble (due to the presence of non-standard effects), i.e,  $H(z_f) = H_{\text{rad}}(z_f) f(z_f, z_r, n)$ , effective annihilation cross-section from Eq. ((A.3)) and approximated form of the number density of the dark matter particle in the above equation we get

$$\left( \frac{g_{\Sigma_1^0}}{\pi^2} M_{\Sigma_1}^3 z_f^{-3/2} e^{-z_f} \right) \left( \frac{111}{36} \frac{\pi \alpha_L^2}{M_{\Sigma_1}^2} \right) = \left( 1.66 \sqrt{g_*(T_f)} \frac{1}{M_{pl}} \frac{M_{\Sigma_1}^2}{z_f^2} \right) f(z_f, z_r, n). \quad (\text{B.6})$$

First we put numerical values of the constants ( $g_{\Sigma_1^0}, \alpha_L, M_{pl}, g_*(T_f)$ ) in the above equation. Then a few steps of algebraic manipulations lead us to a much simplified form of the transcendental equation,

$$\begin{aligned} z_f^{1/2} e^{-z_f} &\simeq (6300 \times 10^{-19}) M_{\Sigma_1} f(z_f, z_r, n) \\ \text{or, } z_f &\simeq 35 + \frac{1}{2} \ln z_f - \ln M_{\Sigma_1} - \ln f(z_f, z_r, n) \\ \text{or, } z_f &\simeq 28 + \frac{1}{2} \ln z_f - \ln (M_{\Sigma_1}/1000) - \ln f(z_f, z_r, n), \end{aligned} \quad (\text{B.7})$$

solving which we can get the freeze-out temperature  $T_f = M_{\Sigma_1}/z_f$ .

## C Reaction densities of various decay, inverse decay, scattering processes

Let us consider a generic decay process ( $\psi \rightarrow a + b + \dots$ ) and a scattering process ( $\psi + \chi \rightarrow a + b + \dots$ ) where  $\psi$  is the particle whose abundance is to be tracked. The space-time density of the generic scattering process in thermal equilibrium is expressed as

$$\gamma(\psi + \chi \rightarrow a + b + \dots) = \int d\Pi_\psi d\Pi_\chi f_\psi f_\chi \int d\Pi_a d\Pi_b \dots (2\pi)^4 \delta^4(p_\psi + p_\chi - p_a - p_b - \dots) |\mathcal{M}|^2, \quad (\text{C.1})$$

where  $d\Pi_i = \frac{d^3 p_i}{(2\pi)^3 2E_i}$  is the phase space factor,  $|\mathcal{M}|^2$  is the squared transition amplitude and  $f_i$  is the distribution function of the concerned particle species. For a decay process the above integral can be simplified to express the reaction density as

$$\gamma(\psi \rightarrow a + b) = n_\psi^{eq} \frac{K_1(z)}{K_2(z)} \Gamma_\psi, \quad (\text{C.2})$$

where  $\Gamma_\psi$  is the decay width of  $\psi$  to  $a, b$  in the rest frame of  $\psi$  and  $n_\psi^{eq}$  is the equilibrium number density of the  $\psi$  particle. For the scattering process. For the scattering process the thermally averaged reaction rate can be reduced to

$$\gamma(\psi + \chi \rightarrow a + b) = \frac{T}{64\pi^4} \int_{s_{min}}^{\infty} ds \sqrt{s} K_1 \left( \frac{\sqrt{s}}{T} \right) \hat{\sigma}(s), \quad (\text{C.3})$$

where the integration is evaluated over the centre of mass energy ( $s$ ), whose minimum admissible value is either square of sum of the initial particle masses or final particle masses

(which ever is greater), i.e  $s_{min} = \max [(m_\psi + m_\chi)^2, (m_a + m_b)^2]$ . Here  $\hat{\sigma}(s)$  is the reduced cross-section which is related to the actual cross-section ( $\sigma$ ) of the concerned process through the function<sup>21</sup>  $\lambda$  as

$$\hat{\sigma} = 2s\lambda[1, \frac{m_\psi^2}{s}, \frac{m_\chi^2}{s}]\sigma. \quad (\text{C.4})$$

The integration variable  $s$  in Eq. (C.3) can be replaced by a dimension-less one ( $x = s/m_\psi^2$ ) such that the reaction density of scattering can be expressed as

$$\gamma(\psi + \chi \rightarrow a + b) = \frac{M_\psi^4}{64\pi^4 z} \int_{x_{min}}^{\infty} \sqrt{x} K_1(z\sqrt{x}) \hat{\sigma}(x) dx. \quad (\text{C.5})$$

## D Scattering cross-section of various processes

**Gauge boson mediated scattering process:** Reduced scattering cross-section for the gauge boson mediated processes<sup>22</sup> is given by

$$\hat{\sigma}_A = \frac{6g_{2L}^4}{72\pi} \left[ \frac{45}{2} r(x) - \frac{27}{2} r(x)^3 - \left\{ 9 \left( r(x)^2 - 2 \right) + 18 \left( r(x)^2 - 1 \right)^2 \right\} \ln \left( \frac{1+r(x)}{1-r(x)} \right) \right], \quad (\text{D.1})$$

where  $g_{2L}$  is the  $SU(2)_L$  gauge coupling constant and  $r(x) = \sqrt{1-4/x}$ .

**$\Delta L = 2$  scattering processes:** The off-shell part of the  $\Delta L = 2$  scattering cross-section (for  $s$ -channel process) is given by

$$\begin{aligned} \hat{\sigma}_s(LH \rightarrow \bar{L}H^*) &= \frac{(y_{\Sigma_2}^\dagger y_{\Sigma_2})_{22}^2}{4\pi} \left[ 2 + x D_s^{2sub} + \left( 2 - 3x \frac{m_3}{\tilde{m}_1} \right) \text{Re} \{D_s\} + 3 \frac{m_3}{\tilde{m}_1} \left( x \frac{m_3}{\tilde{m}_1} - 2 \right) \right. \\ &\quad \left. - \frac{2}{x} \ln(1+x) \left\{ 1 + \left( \text{Re} \{D_s\} + 3 \frac{m_3}{\tilde{m}_1} \right) (1+x) \right\} \right] \end{aligned} \quad (\text{D.2})$$

where  $D_s$  is the  $s$  channel propagator given by

$$D_s = \frac{1}{s - M_{\Sigma_2}^2 + i\Gamma_{\Sigma_2} M_{\Sigma_2}} \quad (\text{D.3})$$

and  $D_s^{2sub}$  is the modulus square of ‘resonance contribution subtracted’  $s$  channel propagator, expressed in terms of  $D_s$  as

$$D_s^{2sub} = 1 - \frac{\pi}{\Gamma_{\Sigma_2} M_{\Sigma_2} |D_s|^2} \delta(s - M_{\Sigma_2}^2). \quad (\text{D.4})$$

Cross-section for the  $t$  channel process is given by

$$\hat{\sigma}_t(LL \rightarrow H^*H^*) = \frac{(y_{\Sigma_2}^\dagger y_{\Sigma_2})_{22}^2}{2\pi} \left[ \frac{3x}{2} \left( \frac{m_3^2}{\tilde{m}_1^2} + \frac{2}{1+x} \right) + \left( 3 \frac{m_3}{\tilde{m}_1} - \frac{3}{2+x} \right) \ln(1+x) \right] \quad (\text{D.5})$$

<sup>21</sup> $\lambda[x_1, x_2, x_3] = (x_1 - x_2 - x_3)^2 - 4x_2x_3$

<sup>22</sup>It includes  $\Sigma, \Sigma \rightarrow$  all possible fermion doublets, Higgs, gauge bosons

## References

- [1] Y. Sofue and V. Rubin, *Rotation curves of spiral galaxies*, *Ann. Rev. Astron. Astrophys.* **39** (2001) 137 [[astro-ph/0010594](#)].
- [2] M. Bartelmann and P. Schneider, *Weak gravitational lensing*, *Phys. Rept.* **340** (2001) 291 [[astro-ph/9912508](#)].
- [3] D. Clowe, A. Gonzalez and M. Markevitch, *Weak lensing mass reconstruction of the interacting cluster 1E0657-558: Direct evidence for the existence of dark matter*, *Astrophys. J.* **604** (2004) 596 [[astro-ph/0312273](#)].
- [4] WMAP collaboration, *Nine-Year Wilkinson Microwave Anisotropy Probe (WMAP) Observations: Final Maps and Results*, *Astrophys. J. Suppl.* **208** (2013) 20 [[1212.5225](#)].
- [5] PLANCK collaboration, *Planck 2015 results. XIII. Cosmological parameters*, *Astron. Astrophys.* **594** (2016) A13 [[1502.01589](#)].
- [6] PLANCK collaboration, *Planck 2018 results. VI. Cosmological parameters*, *Astron. Astrophys.* **641** (2020) A6 [[1807.06209](#)].
- [7] V. Silveira and A. Zee, *SCALAR PHANTOMS*, *Phys. Lett. B* **161** (1985) 136.
- [8] R. J. Scherrer and M. S. Turner, *On the Relic, Cosmic Abundance of Stable Weakly Interacting Massive Particles*, *Phys. Rev. D* **33** (1986) 1585.
- [9] M. Srednicki, R. Watkins and K. A. Olive, *Calculations of Relic Densities in the Early Universe*, *Nucl. Phys. B* **310** (1988) 693.
- [10] P. Gondolo and G. Gelmini, *Cosmic abundances of stable particles: Improved analysis*, *Nucl. Phys. B* **360** (1991) 145.
- [11] L. J. Hall, K. Jedamzik, J. March-Russell and S. M. West, *Freeze-In Production of FIMP Dark Matter*, *JHEP* **03** (2010) 080 [[0911.1120](#)].
- [12] A. Biswas, D. Majumdar and P. Roy, *Nonthermal two component dark matter model for Fermi-LAT  $\gamma$ -ray excess and 3.55 keV X-ray line*, *JHEP* **04** (2015) 065 [[1501.02666](#)].
- [13] N. Bernal, M. Heikinheimo, T. Tenkanen, K. Tuominen and V. Vaskonen, *The Dawn of FIMP Dark Matter: A Review of Models and Constraints*, *Int. J. Mod. Phys. A* **32** (2017) 1730023 [[1706.07442](#)].
- [14] K. Petraki and R. R. Volkas, *Review of asymmetric dark matter*, *Int. J. Mod. Phys. A* **28** (2013) 1330028 [[1305.4939](#)].
- [15] B. Carr and F. Kuhnel, *Primordial black holes as dark matter candidates*, *SciPost Phys. Lect. Notes* **48** (2022) 1 [[2110.02821](#)].
- [16] B. Pontecorvo, *Neutrino Experiments and the Problem of Conservation of Leptonic Charge*, *Zh. Eksp. Teor. Fiz.* **53** (1967) 1717.
- [17] V. N. Gribov and B. Pontecorvo, *Neutrino astronomy and lepton charge*, *Phys. Lett. B* **28** (1969) 493.
- [18] T2K collaboration, *Measurement of neutrino and antineutrino oscillations by the T2K experiment including a new additional sample of  $\nu_e$  interactions at the far detector*, *Phys. Rev. D* **96** (2017) 092006 [[1707.01048](#)].
- [19] T2K collaboration, *Search for CP Violation in Neutrino and Antineutrino Oscillations by the T2K Experiment with  $2.2 \times 10^{21}$  Protons on Target*, *Phys. Rev. Lett.* **121** (2018) 171802 [[1807.07891](#)].
- [20] NOvA collaboration, *Constraints on Oscillation Parameters from  $\nu_e$  Appearance and  $\nu_\mu$  Disappearance in NOvA*, *Phys. Rev. Lett.* **118** (2017) 231801 [[1703.03328](#)].



- [21] NOvA collaboration, *New constraints on oscillation parameters from  $\nu_e$  appearance and  $\nu_\mu$  disappearance in the NOvA experiment*, *Phys. Rev. D* **98** (2018) 032012 [[1806.00096](#)].
- [22] DAYA BAY collaboration, *Measurement of the Electron Antineutrino Oscillation with 1958 Days of Operation at Daya Bay*, *Phys. Rev. Lett.* **121** (2018) 241805 [[1809.02261](#)].
- [23] RENO collaboration, *Measurement of Reactor Antineutrino Oscillation Amplitude and Frequency at RENO*, *Phys. Rev. Lett.* **121** (2018) 201801 [[1806.00248](#)].
- [24] MINOS collaboration, *Measurement of Neutrino and Antineutrino Oscillations Using Beam and Atmospheric Data in MINOS*, *Phys. Rev. Lett.* **110** (2013) 251801 [[1304.6335](#)].
- [25] DOUBLE CHOOZ collaboration, *Improved measurements of the neutrino mixing angle  $\theta_{13}$  with the Double Chooz detector*, *JHEP* **10** (2014) 086 [[1406.7763](#)].
- [26] I. Esteban, M. C. Gonzalez-Garcia, A. Hernandez-Cabezudo, M. Maltoni and T. Schwetz, *Global analysis of three-flavour neutrino oscillations: synergies and tensions in the determination of  $\theta_{23}$ ,  $\delta_{CP}$ , and the mass ordering*, *JHEP* **01** (2019) 106 [[1811.05487](#)].
- [27] P. Minkowski,  *$\mu \rightarrow e\gamma$  at a Rate of One Out of  $10^9$  Muon Decays?*, *Phys. Lett. B* **67** (1977) 421.
- [28] M. Gell-Mann, P. Ramond and R. Slansky, *Complex Spinors and Unified Theories*, *Conf. Proc. C* **790927** (1979) 315 [[1306.4669](#)].
- [29] T. Yanagida, *Horizontal Symmetry and Masses of Neutrinos*, *Prog. Theor. Phys.* **64** (1980) 1103.
- [30] R. N. Mohapatra and G. Senjanovic, *Neutrino Mass and Spontaneous Parity Nonconservation*, *Phys. Rev. Lett.* **44** (1980) 912.
- [31] R. Foot, H. Lew, X. G. He and G. C. Joshi, *Seesaw Neutrino Masses Induced by a Triplet of Leptons*, *Z. Phys. C* **44** (1989) 441.
- [32] E. Ma, *Pathways to naturally small neutrino masses*, *Phys. Rev. Lett.* **81** (1998) 1171 [[hep-ph/9805219](#)].
- [33] M. Fukugita and T. Yanagida, *Baryogenesis Without Grand Unification*, *Phys. Lett. B* **174** (1986) 45.
- [34] E. Ma and D. Suematsu, *Fermion Triplet Dark Matter and Radiative Neutrino Mass*, *Mod. Phys. Lett. A* **24** (2009) 583 [[0809.0942](#)].
- [35] J. Hisano, S. Matsumoto and M. M. Nojiri, *Explosive dark matter annihilation*, *Phys. Rev. Lett.* **92** (2004) 031303 [[hep-ph/0307216](#)].
- [36] J. Hisano, S. Matsumoto, M. M. Nojiri and O. Saito, *Non-perturbative effect on dark matter annihilation and gamma ray signature from galactic center*, *Phys. Rev. D* **71** (2005) 063528 [[hep-ph/0412403](#)].
- [37] A. Biswas, D. Borah and D. Nanda, *When Freeze-out Precedes Freeze-in: Sub-TeV Fermion Triplet Dark Matter with Radiative Neutrino Mass*, *JCAP* **09** (2018) 014 [[1806.01876](#)].
- [38] S. Choubey, S. Khan, M. Mitra and S. Mondal, *Singlet-Triplet Fermionic Dark Matter and LHC Phenomenology*, *Eur. Phys. J. C* **78** (2018) 302 [[1711.08888](#)].
- [39] C. Cosme, M. Dutra, T. Ma, Y. Wu and L. Yang, *Neutrino portal to FIMP dark matter with an early matter era*, *JHEP* **03** (2021) 026 [[2003.01723](#)].
- [40] J. A. Evans, A. Ghalsasi, S. Gori, M. Tammara and J. Zupan, *Light Dark Matter from Entropy Dilution*, *JHEP* **02** (2020) 151 [[1910.06319](#)].
- [41] A. Biswas, D. K. Ghosh and D. Nanda, *Concealing Dirac neutrinos from cosmic microwave background*, *JCAP* **10** (2022) 006 [[2206.13710](#)].
- [42] D. Borah, S. Jyoti Das, A. K. Saha and R. Samanta, *Probing WIMP dark matter via gravitational waves' spectral shapes*, *Phys. Rev. D* **106** (2022) L011701 [[2202.10474](#)].

- [43] S. Tsujikawa, *Quintessence: A Review*, *Class. Quant. Grav.* **30** (2013) 214003 [[1304.1961](#)].
- [44] P. G. Ferreira and M. Joyce, *Cosmology with a primordial scaling field*, *Phys. Rev. D* **58** (1998) 023503 [[astro-ph/9711102](#)].
- [45] Y. Gouttenoire, G. Servant and P. Simakachorn, *Kination cosmology from scalar fields and gravitational-wave signatures*, [2111.01150](#).
- [46] P. Salati, *Quintessence and the relic density of neutralinos*, *Phys. Lett. B* **571** (2003) 121 [[astro-ph/0207396](#)].
- [47] S. Profumo and P. Ullio, *SUSY dark matter and quintessence*, *JCAP* **11** (2003) 006 [[hep-ph/0309220](#)].
- [48] F. D’Eramo, N. Fernandez and S. Profumo, *When the Universe Expands Too Fast: Relentless Dark Matter*, *JCAP* **05** (2017) 012 [[1703.04793](#)].
- [49] S. Nojiri and S. D. Odintsov, *Unified cosmic history in modified gravity: from  $F(R)$  theory to Lorentz non-invariant models*, *Phys. Rept.* **505** (2011) 59 [[1011.0544](#)].
- [50] R. Catena, N. Fornengo, A. Masiero, M. Pietroni and M. Schelke, *Enlarging  $mSUGRA$  parameter space by decreasing pre-BBN Hubble rate in Scalar-Tensor Cosmologies*, *JHEP* **10** (2008) 003 [[0712.3173](#)].
- [51] N. Okada and S. Okada, *Gauss-Bonnet braneworld cosmological effect on relic density of dark matter*, *Phys. Rev. D* **79** (2009) 103528 [[0903.2384](#)].
- [52] M. T. Meehan and I. B. Whittingham, *Dark matter relic density in Gauss-Bonnet braneworld cosmology*, *JCAP* **12** (2014) 034 [[1404.4424](#)].
- [53] S. Nojiri, S. D. Odintsov and V. K. Oikonomou, *Modified Gravity Theories on a Nutshell: Inflation, Bounce and Late-time Evolution*, *Phys. Rept.* **692** (2017) 1 [[1705.11098](#)].
- [54] A. Biswas, A. Kar, B.-H. Lee, H. Lee, W. Lee, S. Scopel et al., *WIMPs in Dilatonic Einstein Gauss-Bonnet Cosmology*, [2303.05813](#).
- [55] F. D’Eramo, N. Fernandez and S. Profumo, *Dark Matter Freeze-in Production in Fast-Expanding Universes*, *JCAP* **02** (2018) 046 [[1712.07453](#)].
- [56] A. Biswas, D. Borah and D. Nanda, *keV Neutrino Dark Matter in a Fast Expanding Universe*, *Phys. Lett. B* **786** (2018) 364 [[1809.03519](#)].
- [57] S. Ganguly, S. Roy and A. Tapadar, *Secluded dark sector and muon ( $g-2$ ) in the light of fast expanding Universe*, *JCAP* **02** (2023) 044 [[2208.13608](#)].
- [58] D. K. Ghosh, S. Jeusun and D. Nanda, *Long-lived inert Higgs boson in a fast expanding universe and its imprint on the cosmic microwave background*, *Phys. Rev. D* **106** (2022) 115001 [[2206.04940](#)].
- [59] G. Arcadi, J. P. Neto, F. S. Queiroz and C. Siqueira, *Roads for right-handed neutrino dark matter: Fast expansion, standard freeze-out, and early matter domination*, *Phys. Rev. D* **105** (2022) 035016 [[2108.11398](#)].
- [60] B. Barman, P. Ghosh, F. S. Queiroz and A. K. Saha, *Scalar multiplet dark matter in a fast expanding Universe: Resurrection of the desert region*, *Phys. Rev. D* **104** (2021) 015040 [[2101.10175](#)].
- [61] S.-L. Chen, A. Dutta Banik and Z.-K. Liu, *Leptogenesis in fast expanding Universe*, *JCAP* **03** (2020) 009 [[1912.07185](#)].
- [62] D. Mahanta and D. Borah, *TeV Scale Leptogenesis with Dark Matter in Non-standard Cosmology*, *JCAP* **04** (2020) 032 [[1912.09726](#)].

- [63] P. Konar, A. Mukherjee, A. K. Saha and S. Show, *A dark clue to seesaw and leptogenesis in a pseudo-Dirac singlet doublet scenario with (non)standard cosmology*, *JHEP* **03** (2021) 044 [[2007.15608](#)].
- [64] Z.-F. Chang, Z.-X. Chen, J.-S. Xu and Z.-L. Han, *FIMP Dark Matter from Leptogenesis in Fast Expanding Universe*, *JCAP* **06** (2021) 006 [[2104.02364](#)].
- [65] M. Chakraborty and S. Roy, *Baryon asymmetry and lower bound on right handed neutrino mass in fast expanding Universe: an analytical approach*, *JCAP* **11** (2022) 053 [[2208.04046](#)].
- [66] D. Mahanta and D. Borah, *WIMPy Leptogenesis in Non-Standard Cosmologies*, [2208.11295](#).
- [67] A. Di Marco, A. D. Banik, A. Ghoshal and G. Pradisi, *Minimal Leptogenesis in Brane-inspired Cosmology*, [2211.11361](#).
- [68] T. Hambye, Y. Lin, A. Notari, M. Papucci and A. Strumia, *Constraints on neutrino masses from leptogenesis models*, *Nucl. Phys. B* **695** (2004) 169 [[hep-ph/0312203](#)].
- [69] D. Aristizabal Sierra, J. F. Kamenik and M. Nemevsek, *Implications of Flavor Dynamics for Fermion Triplet Leptogenesis*, *JHEP* **10** (2010) 036 [[1007.1907](#)].
- [70] T. Hambye, *Leptogenesis: beyond the minimal type I seesaw scenario*, *New J. Phys.* **14** (2012) 125014 [[1212.2888](#)].
- [71] D. Vatsyayan and S. Goswami, *Lowering the scale of fermion triplet leptogenesis with two Higgs doublets*, *Phys. Rev. D* **107** (2023) 035014 [[2208.12011](#)].
- [72] FERMI-LAT collaboration, *The Large Area Telescope on the Fermi Gamma-ray Space Telescope Mission*, *Astrophys. J.* **697** (2009) 1071 [[0902.1089](#)].
- [73] M. Cirelli, N. Fornengo and A. Strumia, *Minimal dark matter*, *Nucl. Phys. B* **753** (2006) 178 [[hep-ph/0512090](#)].
- [74] G. Bélanger, S. Choubey, R. M. Godbole, S. Khan, M. Mitra and A. Roy, *WIMP and FIMP dark matter in singlet-triplet fermionic model*, *JHEP* **11** (2022) 133 [[2208.00849](#)].
- [75] LZ collaboration, *First Dark Matter Search Results from the LUX-ZEPLIN (LZ) Experiment*, [2207.03764](#).
- [76] J. Hisano, K. Ishiwata, N. Nagata and T. Takesako, *Direct Detection of Electroweak-Interacting Dark Matter*, *JHEP* **07** (2011) 005 [[1104.0228](#)].
- [77] MAGIC, FERMI-LAT collaboration, *Limits to Dark Matter Annihilation Cross-Section from a Combined Analysis of MAGIC and Fermi-LAT Observations of Dwarf Satellite Galaxies*, *JCAP* **02** (2016) 039 [[1601.06590](#)].
- [78] R. K. Leane, T. R. Slatyer, J. F. Beacom and K. C. Y. Ng, *GeV-scale thermal WIMPs: Not even slightly ruled out*, *Phys. Rev. D* **98** (2018) 023016 [[1805.10305](#)].
- [79] ATLAS collaboration, *Search for long-lived charginos based on a disappearing-track signature using  $136\text{ fb}^{-1}$  of  $pp$  collisions at  $\sqrt{s} = 13\text{ TeV}$  with the ATLAS detector*, *Eur. Phys. J. C* **82** (2022) 606 [[2201.02472](#)].
- [80] A. Dainese, M. Mangano, A. B. Meyer, A. Nisati, G. Salam and M. A. Vesterinen, eds., *Report on the Physics at the HL-LHC, and Perspectives for the HE-LHC*, vol. 7/2019 of CERN Yellow Reports: Monographs. CERN, Geneva, Switzerland, 2019, [10.23731/CYRM-2019-007](#).
- [81] K. Griest and D. Seckel, *Three exceptions in the calculation of relic abundances*, *Phys. Rev. D* **43** (1991) 3191.
- [82] C. Pitrou, A. Coc, J.-P. Uzan and E. Vangioni, *Precision big bang nucleosynthesis with improved Helium-4 predictions*, *Phys. Rept.* **754** (2018) 1 [[1801.08023](#)].
- [83] G. Mangano, G. Miele, S. Pastor, T. Pinto, O. Pisanti and P. D. Serpico, *Relic neutrino decoupling including flavor oscillations*, *Nucl. Phys. B* **729** (2005) 221 [[hep-ph/0506164](#)].

- [84] P. F. de Salas and S. Pastor, *Relic neutrino decoupling with flavour oscillations revisited*, *JCAP* **07** (2016) 051 [[1606.06986](#)].
- [85] J. Hisano, S. Matsumoto, M. Nagai, O. Saito and M. Senami, *Non-perturbative effect on thermal relic abundance of dark matter*, *Phys. Lett. B* **646** (2007) 34 [[hep-ph/0610249](#)].
- [86] V. A. Kuzmin, V. A. Rubakov and M. E. Shaposhnikov, *On the Anomalous Electroweak Baryon Number Nonconservation in the Early Universe*, *Phys. Lett. B* **155** (1985) 36.
- [87] S. Davidson and A. Ibarra, *A Lower bound on the right-handed neutrino mass from leptogenesis*, *Phys. Lett. B* **535** (2002) 25 [[hep-ph/0202239](#)].
- [88] L. Covi, E. Roulet and F. Vissani, *CP violating decays in leptogenesis scenarios*, *Phys. Lett. B* **384** (1996) 169 [[hep-ph/9605319](#)].
- [89] D. Baumann, *Inflation*, in *Theoretical Advanced Study Institute in Elementary Particle Physics: Physics of the Large and the Small*, pp. 523–686, 2011, DOI [[0907.5424](#)].